Effects of Vorticity on Rocket Combustion Stability

G. A. Flandro*

University of Tennessee Space Institute, Tullahoma, Tennessee 37388-8897

Combustion stability computations are currently based on an irrotational model that allows slip flow at the burning surface. However, the no-slip boundary condition must be satisfied when gas motions are parallel to the combustion zone. Then waves of vorticity are created that distort the acoustic wave structure and modify the fluctuating normal velocity component upon which system stability is so strongly dependent. This flow problem is solved here in analytical form to bring the physical details into focus. Crocco's theorem shows that the creation of vorticity is due primarily to the axial unsteady pressure gradient across mean flow streamlines at the surface. Hence, there is a transfer of energy from the pressure oscillations (acoustic field) to the rotational waves (vorticity field). It is in this interaction that the incoming flow acquires the axial motion of the acoustic wave. Stability calculations based on this model yield the three-dimensional form of Culick's one-dimensional flow-turning correction and clarify its origin. However, continuity at the burning surface requires a correction to the radial velocity fluctuations. Incorporation of this new driving effect leads to a motor system that is significantly less stable than in the classical prediction (Standard Stability Prediction Program) for some configurations.

Nomenclature

A_b	= boundary acoustic admittance function, complex number
a_0	= mean speed of sound
E_m^2	= normalization constant for mode m
e_r, e_θ, e_z	= unit vectors in radial, transverse, and axial directions
h_0	= total enthalpy
k	= general acoustic wave number, $k_m + \mathbb{O}(M_b) = k_m + M_b k_\alpha$
k_m	= wave number for axial mode m
k_α	= correction to wave number, $(\omega_m + i\alpha_m)/M_b$
L	= chamber length
M_b	= mean flow Mach number
m	= mode index
n	= outward pointing unit normal vector
P_0	= mean chamber pressure
p	= pressure
R	= chamber radius
R_b, R_v	= response functions
r	= radial position
S	= azimuthal part of vector potential
S	= vector potential function for rotational motion
t	= time
U_r, U_z	= mean flow velocity component
U	= mean flow velocity vector, $U_r e_r + U_z e_z$
u'	= oscillatory velocity vector amplitude, $u^{(1)}(r, t)$ $= u' \exp(-ikt), u'e_r + w'e_z$
y	= radial distance from boundary, $1 - r$
z	= axial position
α	= growth rate, dimensional, s^{-1}
γ	= ratio of specific heats
δ	= inverse square root of acoustic Reynolds number, $\sqrt{\nu/a_0 L}$
ε	= wave amplitude
ζ'	= vorticity function, ω'/r
η	= stretched radial coordinate for viscous solution, y/δ
λ	= characteristic ratio or "injection parameter," M_b/k_m
ν	= kinematic viscosity, μ/ρ
ξ	= stretched radial coordinate for inviscid solution, y/λ
ρ	= density
ϕ	= velocity potential for irrotational motion, acoustic wave
$\chi(r, z)$	= vorticity spatial distribution function
ψ	= complex exponential argument, $\psi^{(r)} + i\psi^{(i)}$
Ω	= mean vorticity amplitude, $\Omega = \Omega e_\theta$
ω'	= amplitude of vorticity fluctuation

Subscripts

b	= conditions at the combustion zone
C	= pressure coupling effects, response function form
FD	= frictional damping effects at burning surface
FT	= flow-turning effects
m	= mode integer in wave number, $k_m = m\pi R/L$
N	= nozzle effects
P	= particulate damping effects
R	= rotational flow driving effects
r	= radial component
V	= viscous attenuation at inert surfaces
VC	= velocity coupling effects
VI	= mean flow interaction effects
z	= axial component
θ	= azimuthal component
0	= stagnation value of quantity

I. Introduction

AN oft-repeated scenario is that a solid propellant rocket motor predicted to be stable by application of the standard stability prediction program (SSPP)[1,2] exhibits serious longitudinal mode instability in qualification testing. No indication of impending difficulties appears until after full-scale motor firings have commenced. Ad hoc design modifications to eliminate or minimize the oscillatory behavior are expensive and disruptive of the development process.

Classical methods for rocket motor combustion stability computations are based on an irrotational acoustic model that does not explicitly account for vortical flow effects.[1-5] Oscillatory slip flow is allowed at the burning surface. Such approximations are based on the notion that viscous stresses and related vorticity transport are negligible due to the strong surface blowing. Difficulties with this method as a predictive tool, especially in cases involving longitudinal oscillations with gas fluctuations parallel to the burning surface, motivated the formulation of corrections such as the classical flow-turning and velocity coupling terms.[5-9] Several attempts have been made, without clear-cut success, to establish the validity of the correction terms by additional theoretical work[10] and by experiments.[11,12]

Culick's one-dimensional analysis,[7] which gives rise to the important flow-turning correction, assumed that the unsteady gas motion was normal at the propellant boundary. This is not a requirement imposed by the mathematical protocol of the analytical method. This choice of boundary condition is a major departure from the philosophy of the original multidimensional theory, which places no restrictions on the velocity component parallel to the burning surface. It is significant that this important damping term does not appear in the three-dimensional combustion instability theory. The latter is therefore corrected by simply "patching" the one-dimensional result.[8]

This motivated Flandro[13] to employ acoustic boundary-layer theory to determine corrections to the stability algorithm based on the idea that the flow-turning energy loss must arise as the result of the no-slip boundary condition in the one-dimensional calculations. This approach demonstrated both the importance of vorticity effects and a significant influence on system stability. The results were not correctly interpreted because of the thin acoustic boundary-layer assumption. In fact, as will be shown in detail in this article, unsteady vorticity modifies the entire flowfield rather than just a thin surface layer. Use of the terminology "acoustic boundary layer" is therefore inappropriate, except in very high-frequency oscillations or at inert surfaces.

The boundary-layer assumption also led to application of a simplified model of the chamber mean flow. On this basis, other investigators concluded that the theory could not account for interactions between the irrotational acoustic waves and the rotational flowfield within the chamber volume. For example, Culick and Yang[14] state that acoustic boundary-layer corrections are distinct from the flow-turning effect. However, it will be demonstrated in detail in this article that flow-turning is a direct consequence of the physical requirement that gas particles enter the chamber normal to the boundary with the attendant production of vorticity at the burning surface. Therefore, all information needed to compute the flow-turning loss (and other important flow interactions not studied previously) is contained in the earlier theory.[13]

Recent experimental[15-17] and numerical work[18-24] verify that acoustic motions parallel to a burning propellant surface must be accompanied by vorticity waves that modify the acoustic wave structure in a dramatic way as predicted analytically.[13] It will be shown in what follows that unsteady vorticity is created as gas particles emerging from the burning zone cross the fluctuating axial acoustic pressure gradient. This is a direct consequence of the Crocco–Vazsonyi theorem. Analogous physical processes account for the vorticity that dominates the mean flowfield in the familiar model by Culick.[25-27]

Rotational flow effects must be accounted for in rocket motor stability computations, since they bring about not only a radical distortion of the acoustic mode shapes, but also important modifications of the radial velocity fluctuations at the burning surface. The simple admittance (or response function) used in previous stability computations[1-8] is not a sufficiently complete statement of the boundary conditions. The system fluctuating energy balance is dependent on both chemical and fluid dynamic response to incident wave motions. The presence of vorticity introduces interactions that cannot be represented using simple acoustic admittance boundary conditions.

II. Approach

It is the goal of the work described herein to clarify the role played by vorticity production and propagation on the stability of combustion gas oscillations in a three-dimensional rocket chamber. We seek a closed-form analytical solution comparable in mathematical quality to the original irrotational, three-dimensional combustion stability model. However, to improve on what has already been done, it is necessary to incorporate rotational flow effects and satisfy physically correct boundary conditions. The phrases "rotational flow" and "flow with vorticity" (or "vortical flow") have identical meaning and are used interchangeably throughout what follows. We are not referring here to vortex shedding phenomena, which represent a separate, but related, type of flow coupling.[28-30]

As usual, completely general three-dimensional, time-dependent, analytical solutions of the Navier–Stokes equations

do not come easily to hand. This is true even for the mean flow. Culick's earlier successful work with the steady flowfield[25] demonstrates the correct approach; namely, restriction of the basic analysis to a simple but realistic geometry such as a cylindrical chamber. In that work, careful attention to vorticity transport was the key to success. This approach is extended in this article to the analogous unsteady problem.

Emphasis throughout this work is on enhanced physical understanding by means of careful application of analytical techniques. This precludes dependence on strictly computational methods as used by others.[18–24] Also, because of accuracy limitations, artificial diffusion, and other difficulties inherent in numerical solutions of the Navier–Stokes equations, it is difficult to deal quantitatively with the system stability properties, although there has apparently been some recent success.[21] Therefore, as much as possible is carried out in analytical form.

The analysis begins with the same set of differential equations describing the time-dependent flow system used in earlier efforts. Both inviscid and viscous cases are considered. Two key differences in approach are introduced. The first is careful evaluation of rotational flow terms that are dropped in previous models. The second is a careful reassessment of the boundary conditions, especially those near the burning surface. The practice of using only the admittance function or response function (pressure coupling with an empirically defined velocity coupling) to represent the surface conditions is questioned in this article. New terms are identified that were lost in previous acoustics models. Their existence is readily established by careful attention to basic surface mass and momentum balances in both the acoustics and the rotational flow corrections.

The first step is a review of successful steady flow models. This yields insight into the origin of vorticity in the injection driven flowfields. The acoustic solution is then extended to first-order in the mean flow Mach number to check certain assumptions used in earlier work. A careful study is then made of the unsteady vorticity. It is demonstrated that these effects are certainly not "of second-order" as assumed by some analysts. The new flowfield results are then incorporated into a careful reassessment of the system stability properties.

The validity of the solutions is established by comparison to the recent cold-flow experimental data of Brown, Shaeffer, and their co-workers.[15,16] Excellent agreement is demonstrated without adjustment of any physical or geometrical parameters describing the test configuration. Finite difference numerical integration of the full set of governing equations by Roach[19] was also used to verify the analytical results.

III. Analysis

The analysis begins with a set of equations identical to the initial set used in the previous models of combustion stability. Since vorticity is to be the focus, care is taken to utilize the appropriate notation in the convective acceleration terms and related expressions in order that the rotational flow effects are not lost. The assumption of irrotational flow made in treating the gas oscillations as simple acoustic waves is carefully avoided.

A standard set of dimensionless variables is employed. Velocities are made dimensionless with respect to the chamber sound speed α_0 to emphasize the central role of compressibility in the oscillating field. Lengths are referenced to the chamber radius R mainly for convenience in plotting radial distributions of results. The acoustic wavelength expressions then contain the chamber length-to-radius ratio since longitudinal oscillations will be of primary concern. Time is made dimensionless by dividing by the characteristic time represented by the ratio R/a_0. Pressure is normalized by γP_0, and other thermodynamic variables are nondimensionalized with respect to the chamber stagnation properties.

A. Formulation, Assumptions, and Strategy

The first stage of the analysis is to separate the steady and unsteady parts of the problem. Separation of the two fields is accomplished by writing each variable as the sum of a steady and an unsteady part. It is useful to expand the unsteady part as a perturbation series using powers of the wave amplitude ε as the asymptotic sequence. A second small parameter, the mean flow Mach number at the burning surface M_b is used in further expansions. The principal variables (pressure and velocity vector) are then written as

$$p = \underbrace{1/\gamma + M_b^2 P + \mathbb{O}(M_b^4)}_{\text{steady part}} + \underbrace{\varepsilon p^{(1)} + \varepsilon^2 p^{(2)} + \mathbb{O}(\varepsilon^3)}_{\text{unsteady part}} \quad (1)$$

$$u = \underbrace{M_b U + \mathbb{O}(M_b^2)}_{\text{steady part}} + \underbrace{\varepsilon u^{(1)} + \varepsilon^2 u^{(2)} + \mathbb{O}(\varepsilon^3)}_{\text{unsteady part}} \quad (2)$$

where higher-order corrections may be appended as indicated. Vector U represents the geometry of the mean flowfield. P is a correction to the uniform mean pressure distribution.[27] The superscripts denote the order of the approximation in terms of the wave amplitude. The analysis discussed here accounts only for linear effects in wave amplitude; however, some attention to nonlinear effects in the Mach number will be required in order to achieve physical understanding of critical radial velocity boundary conditions.

These expansions allow separation of the steady and unsteady flows. The steady, inviscid mean flowfield is governed by the continuity and momentum equations

$$\nabla \cdot U = 0 \quad (3)$$

$$\nabla \frac{U \cdot U}{2} - U \times \nabla \times U = -\nabla P \quad (4)$$

and the unsteady flow to first-order in amplitude is represented by the continuity and momentum equations

$$\frac{\partial p^{(1)}}{\partial t} = -\nabla \cdot u^{(1)} - M_b U \cdot \nabla p^{(1)} \quad (5)$$

$$\frac{\partial u^{(1)}}{\partial t} = -\nabla^{(1)} p - M_b[\nabla(u^{(1)} \cdot U) - u^{(1)}$$
$$\times \nabla \times U - U \times \nabla \times u^{(1)}] - \delta^2 \nabla \times \nabla \times u^{(1)} \quad (6)$$

where the standard assumptions[1–8] regarding the thermodynamic variables have been employed and body force terms are not displayed. It is well known[25,26] that viscous forces do not affect the injection-driven mean flow in chambers of typical slenderness ratio L/R and can be dropped without noticeable effect.

B. Review of Mean Flow Solutions with Vorticity

Much depends on a clear understanding of the interactions between the mean and unsteady flows. Therefore, a brief but careful review of the steady flow model is essential. Culick[25] devised an axisymmetric mean flow model that eliminates the deficiencies arising from neglect of vorticity. This steady flow model has been verified experimentally both in cold-flow experiments[26] and in numerical solutions.[19,24]

The Culick mean flow model in the present notation is

$$U = U_r e_r + U_z e_z = -r^{-1} \sin(\tfrac{1}{2}\pi r^2) e_r + \pi z \cos(\tfrac{1}{2}\pi r^2) e_z \quad (7)$$

$$P = -\tfrac{1}{2}[\sin^2(\tfrac{1}{2}\pi r^2)/r^2 + \pi^2 z^2] \qquad (8)$$

$$\Omega = \Omega e_\theta = \pi^2 rz\,\sin(\tfrac{1}{2}\pi r^2)e_\theta \qquad (9)$$

where P is the correction [of $\mathcal{O}(M_b^2)$ in Eq. (1)] to the mean pressure from an analysis by Flandro.[27] Ω is the magnitude of the mean vorticity vector. The vorticity arises from the restriction that a slip flow is not allowed at the injection surface; the flow must enter the chamber in the radially inward direction with no axial component. The origin of the vorticity is often described as a "viscous process" at the boundary,[8] but this proposition requires closer examination in order that analogous processes in the unsteady flow calculations can be properly accounted for. Viscous forces are negligibly small because there are no steep velocity gradients in the mean flow.

The matter is clarified by application of the Crocco–Vazsonyi theorem. For a steady, inviscid flow, the momentum balance, Eq. (4), leads to

$$U \times \Omega = \nabla\{P + [(U \cdot U)/2]\} = \nabla h_0 \qquad (10)$$

where h_0 is the total enthalpy since isentropic flow is assumed. This shows that vorticity will be present if there is a gradient of total enthalpy normal to the streamlines, since

$$U\Omega = \frac{\mathrm{d}h_0}{\mathrm{d}n} \qquad (11)$$

where $\mathrm{d}/\mathrm{d}n$ denotes the rate of change normal to a mean flow streamline, and U is the gas speed. Hence, it is not necessary to invoke viscous effects in the burning zone to explain the vorticity. Gas particles produced by gasification of the solid propellant must have, on average, zero vorticity as they enter the chamber.

Equation (11) shows that vorticity is created as the gas particles cross the axial pressure gradient at the surface, since $U = -1$ and $\mathrm{d}h_0/\mathrm{d}n = \mathrm{d}P/\mathrm{d}z$ at $r = 1$. The vorticity at the surface from Eq. (11) is, therefore,

$$\Omega = -\frac{\partial P}{\partial z} = \pi^2 z \qquad \text{at} \qquad r = 1 \qquad (12)$$

in full agreement with Eq. (9), which was derived in the original analysis without reference to the vorticity boundary conditions.[25] The expression for vorticity shown in Eq. (9) corrects a typographical error in the original paper that indicated the mean vorticity Ω is proportional to π instead of π^2. Vorticity is constant along mean flow streamlines because no viscous forces are present. Propagation of vorticity in the mean flow is controlled by convective rather than diffusive mechanisms.

This information is of crucial importance and guides the unsteady rotational flow calculations. It will be shown that under conditions characterizing most rocket flows, the unsteady flowfield exhibits analogous behavior. In a chamber with longitudinal acoustic oscillations, time-dependent vorticity is created at the surface because the gas particles emerging from the combustion zone must cross the axial acoustic pressure gradient. As is the case with the steady flow, the vorticity is propagated mainly by convection rather than the diffusive mechanisms that dominate classical acoustic boundary-layer behavior. However, viscous corrections may be significant in some situations and will be carefully evaluated.

C. Unsteady Flow with Vorticity

The appropriate starting point in the unsteady analysis is the same set of equations that yields all of the accepted combustion instability results. In order to emphasize the role played by rotational flow effects, all of the standard assumptions will

be retained except those related to vorticity and the boundary condition. For sinusoidal oscillations

$$p^{(1)} = p'\,\exp(-ikt) \qquad (13)$$

$$u^{(1)} = u'\,\exp(-ikt) \qquad (14)$$

$$\omega^{(1)} = \nabla \times u^{(1)} = \omega'\,\exp(-ikt) \qquad (15)$$

where ω' is the vorticity amplitude. The frequency parameter k

$$k = k_m + M_b k_\alpha + \mathcal{O}(M_b^2) \qquad (16)$$

contains a complex part (of order M_b), k_α that accounts for exponential growth or decay of the wave system and frequency corrections. The amplitudes of the sinusoidally varying quantities (denoted by primes) are governed to first-order in wave amplitude by the set

$$ikp' = \nabla \cdot u' + M_b \nabla \cdot p'U \qquad (17)$$

$$iku' = \nabla p' + M_b[\nabla(u' \cdot U) - u' \times \Omega$$
$$- U \times \omega'] + \delta^2 \nabla \times \omega' \qquad (18)$$

where u' and p' are the velocity vector and pressure amplitudes, respectively.

The time-dependent velocity can be broken into a sum of irrotational and rotational parts. Put

$$u' = \hat{u} + \tilde{u} \qquad (19)$$

where the circumflex (^) indicates the acoustic (irrotational) part whereas the tilde (˜) identifies the rotational part. One can at this point choose to "split" Eqs. (17) and (18) into irrotational, compressible (acoustic) and rotational, solenoidal (vortical) parts.[18] Splitting yields the sets

irrotational
$$\begin{cases} \nabla \cdot \hat{u} = ikp' - M_b U \cdot \nabla p' & (20) \\[6pt] ik\hat{u} = \nabla p' + M_b[\nabla(\hat{u}' \cdot U) - (\hat{u}' \times \Omega)] & (21) \end{cases}$$

rotational
$$\begin{cases} \nabla \cdot \tilde{u} = 0 & (22) \\[6pt] ik\tilde{u} = M_b[\nabla(\tilde{u}' \cdot U) - (\tilde{u} \times \Omega) - U \times \omega'] \\[4pt] \qquad + \delta^2 \nabla \times \omega' & (23) \end{cases}$$

The separation is based mainly on the different spatial characteristics of the two wave motions involved. It will be necessary in some parts of the analysis to work with the complete equations, Eqs. (17) and (18). The system stability must be based on the latter coupled set. The splitting idea will be useful in highlighting some important acoustic (irrotational) features of the gas motion on system stability in the next subsection.

D. Combustion Chamber Acoustics—Irrotational Unsteady Gas Oscillations

Much of the past work in combustion stability has been based on an acoustics interpretation of the unsteady gas motion. This is motivated by the experimental fact that the observed frequencies of oscillation are often readily identified with the normal acoustic modes of the combustion chamber. Since there is a vast literature on this subject, only a short discussion is required here. Two key aspects are emphasized. The first is clarification of the velocity boundary conditions at the burning surface from the acoustics standpoint. Certain matters involving conservation of mass require attention. The

second pertains to the relative importance of vorticity effects, again from the standpoint that the chamber motion is dominated by compressibility (acoustics) effects. In the latter regard, the standard stability approach is based on disposing of rotational flow effects. It is necessary to seek the origins of the arguments supporting this neglect and to question their validity.

The set of equations, Eqs. (20) and (21), resulting from dropping rotational terms forms the basis of most acoustic stability calculations. The Mach number is treated as a second small parameter in further perturbation expansion of the equations. A step seldom shown formally in the literature is the insertion of the expressions

$$p' = p_0 + M_b p_1' + \mathbb{O}(M_b^2) \tag{24}$$

$$\hat{u} = \hat{u}_0 + M_b \hat{u}_1 + \mathbb{O}(M_b^2) \tag{25}$$

along with subsequent manipulation of the resulting equations. The corrections of $\mathbb{O}(M_b)$, such as p'_1 and $\hat{u}_1$, are not displayed in the classical literature because they are assumed unimportant in the stability calculations.

An important step in stability calculations is to specify the boundary conditions to be satisfied by the solutions. This is usually handled by introducing an admittance function or response function representing the sensitivity of the combustion process to pressure fluctuations. For example, the approach used in most previous work is to specify that the normal velocity component is given by

$$\mathbf{n} \cdot \hat{u} = -A_b p' + R_v \hat{w} \tag{26}$$

at the burning surfaces.[1–8] R_v is the velocity coupling response function, which is expected to depend on location in the chamber. Similar admittance conditions are specified at the nozzle entrance. Since the normal fluctuating velocity at the surface is the main source of energy driving the wave system, it is essential that the validity of the assumed boundary condition be established, especially from the standpoint of mass conservation. There is no apparent inconsistency in using this boundary condition due to the small size $\mathbb{O}(M_b)$ of the admittance function. However, it is not obvious at the outset that there are not other normal velocity contributions of the same order of magnitude that would be inconsistent with Eq. (26).

These questions can only be answered by extending the acoustics solutions as described. The required relationships are easily found by inserting Eqs. (24) and (25) into (20) and (21), with the result

$$\nabla \cdot \hat{u}_1 = ik_m p_1' + ik_\alpha p_0' - U \cdot \nabla p_0' \tag{27}$$

$$ik_m \hat{u}_1 = \nabla p_1' - ik_\alpha \hat{u}_0 + \nabla(\hat{u}_0 \cdot U) - \hat{u}_0 \times \Omega \tag{28}$$

where p'_0 and $\hat{u}_0$ represent the unperturbed acoustic motion. In the present case, emphasis is on acoustic motions parallel to the burning surface, so the base solution is the acoustic plane wave

$$p_0' = \cos(k_m z) \tag{29}$$

$$\hat{u}_0 = \hat{w}_0 e_z = i \sin(k_m z) e_z \tag{30}$$

where $k_m = m\pi R/L$, and m is the mode integer. Familiar steps[1–8] lead to this solution [combine Eqs. (20) and (21) to form the acoustic wave equation, etc.]. This simple motion describes the most common type of instability involving acoustics of the "organ pipe" variety with oscillations parallel to

the chamber axis. For the plane wave, Eqs. (27) and (28) lead to the three coupled equations

$$ik_m p_1' = \frac{1}{r}\frac{\partial}{\partial r}(r\hat{u}_1) + \frac{\partial \hat{w}_1}{\partial z} - ik_\alpha \cos(k_m z) - k_m U_z \sin(k_m z) \tag{31}$$

$$ik_m \hat{u}_1 = \frac{\partial p_1'}{\partial r} \tag{32}$$

$$ik_m \hat{w}_1 = \frac{\partial p_1'}{\partial z} + k_\alpha \sin(k_m z) + i\frac{\partial U_z}{\partial z}\sin(k_m z)$$
$$+ ik_m U_z \cos(k_m z) \tag{33}$$

for the pressure and velocity component correction terms; the radial and axial velocity corrections are $\hat{u}_1$ and $\hat{w}_1$, respectively. Equations (31–33) are readily solved in terms of known functions: trigonometric, the sine integral (Si), and the entire cosine integral (Chi) functions (see Nomenclature).

Only the solution for the radial velocity correction is needed here in establishing the validity of the boundary condition, Eq. (26). The radial velocity correction is

$$\hat{u}_1 = \left\{ \begin{array}{l} r[2 - (A_b/M_b)]\cos(k_m z) \\ \quad + 2U_r[\cos(k_m z) - R_v k_m z \sin(k_m z)] \\ \quad + k_m^2 r[Si(\pi/2) - Si(\tfrac{1}{2}\pi r^2)]\cos(k_m z) \\ \quad + (2k_m^2/\pi r)[1 - r^2 - \cos(\tfrac{1}{2}\pi r^2)]\cos(k_m z) \end{array} \right\} \tag{34}$$

At the burning surface ($r = 1$), this expression reduces to

$$\hat{u} = \mathbf{n} \cdot \hat{u} = M_b \hat{u}_1 = -A_b \cos(k_m z)$$
$$+ 2M_b R_v k_m z \sin(k_m z) + \mathbb{O}(M_b^2) \tag{35}$$

showing that an interaction term resembling the classical velocity coupling must be present. However, the new term can be traced to the axial pressure gradient rather than the axial velocity fluctutation. It does not involve modification of the combustion process by a "crossflow" velocity at the surface ($w' = 0$ from the no-slip condition). The new effect is mainly the consequence of the density fluctuations in the burning zone. By analogy with the classical velocity coupling, this indicates that the interaction of the fluctuating axial pressure gradient on the combustion processes must either be analyzed or measured. Although it has not been established that existing measurements are useful in setting values for R_v, this interaction is likely to be small. The standard symbol for the velocity coupled response is retained here to minimize the amount of new notation introduced and to emphasize the connection with the classical velocity coupling effect. For example, the new coupling is strongly position-dependent because of the influence of the mean flow as the last terms in Eqs. (31) and (33) show. The stability implications of these findings will be undertaken in Sec. V.

E. Is the Unsteady Vorticity Negligible?

No provision is made in the basic classical stability analysis[1–8] to correct for vorticity propagation. This is based on the assertion that "vorticity effects are of higher order." The origin of this familiar argument opposing the need to include unsteady vorticity corrections is easily demonstrated if one assumes that the unperturbed solution to Eqs. (17) and (18) is an axial plane acoustic wave as described in Eqs. (29) and (30). If effects of vorticity (and viscosity) are assumed unimportant, the motion described should approximate the actual gas motion occupying the main volume of the chamber where any effects of boundary perturbations are minimal and shear stresses approach zero due to symmetry. It is then a simple matter to "prove" the above assertions by computing

the vorticity by taking the curl of the momentum equation, Eq. (18), with the result

$$ik_m\nabla \times u' = ik_m\omega' = -M_b\nabla \times (u' \times \Omega + U \times \omega') \quad (36)$$

Inserting the assumed velocity $u' = \hat{u}$ [from Eq. (30)] and carrying out the operations indicated gives

$$\omega' = -i\frac{1}{k_m}\frac{\partial}{\partial z}(\Omega w')e_\theta = \frac{M_b}{k_m}\pi^2 r \sin(\tfrac{1}{2}\pi r^2)$$

$$\times [\sin(k_m z) + k_m z \cos(k_m z)]e_\theta \quad (37)$$

where higher-order terms have been dropped (e.g., the last term is of the order of the square of the mean Mach number and, hence, can apparently be dropped). The vorticity has only an azimuthal component because of axial symmetry. Equation (37) appears to prove convincingly that the vorticity is of the order of the mean flow Mach number. On this basis, rotational flow effects would not be expected to influence any of the stability calculations, since only first-order unsteady flow properties appear in the linearized stability integrals. Computations of this type suggest that vorticity effects are of no consequence in the linearized stability analysis. The current standard stability calculations (SSPP) are built on this interpretation. More attention to the boundary conditions is required.

F. Other Boundary Conditions—The No-Slip Condition

The base solutions given in Eqs. (29) and (30) cannot represent a realistic solution for the entire combustion chamber. Of greatest concern is that the plane wave velocity, Eq. (30), cannot accommodate the no-slip boundary condition. An idea that has been introduced frequently in the past is that the axial acoustic velocity at the surface can be treated as a cross-flow that scrubs the surface in the combustion zone and produces velocity coupling by interacting with combustion in a manner analogous to the experimentally well-established pressure coupling mechanism. The reality of an effect like velocity coupling is strongly supported by experimental evidence.[9] As demonstrated in Sec. III.D, the axial fluctuating pressure gradient gives rise to a coupling effect that closely resembles what is often called the linear velocity coupling, but without the flow reversal, acoustic erosivity, and other paraphernalia of classical combustion-based velocity coupling.

A more acceptable view is that both steady and unsteady velocity at the surface must be constrained to enter the chamber in the normal direction. Any transverse motion near the surface would occur at the molecular level and would, on average, be zero at the macroscopic level. In other words, the motion of the solid surface itself should be reflected in the near-field average motion of gas particles produced by combustion of that surface. Both steady and unsteady motion of the solid is correctly represented by surface regression normal to the burning boundary. The success of the rotational mean flow solution[25] demonstrates that this is the correct viewpoint. The mean flow is dominated by vorticity created in the manner described by Eq. (12). This is an important hint that it may not be appropriate to neglect the analogous unsteady vorticity, even though Eq. (37) seems to indicate otherwise.

Further insight comes from study of the unsteady boundary conditions. It is useful to use the momentum equation in a manner analogous to its application in the mean flow problem as already discussed. Equation (12) showed that the axial pressure gradient at the injection surface sets the magnitude of the vorticity. The analogous unsteady expression [solve for ω' from the axial component of Eq. (18)] is

$$\omega' = -\frac{1}{M_b}\frac{\partial p'}{\partial z} + \frac{\partial u'}{\partial z} + \pi^2 z u' \quad (38)$$

at $r = 1$. Terms involving the steady and unsteady axial velocities (U_z and w') have been set to zero in accordance with the no-slip requirement. Therefore, Eq. (38) is the equivalent of the no-slip condition. Viscous terms have been suppressed temporarily to emphasize that unsteady vorticity production does not require the presence of viscous shear stresses in the present situation. Viscous effects will be studied later.

The vorticity vector $\omega' = \omega' e_\theta$ has only an azimuthal component due to the assumption of cylindrical symmetry. Since the radial unsteady velocity component u' is small [of the order of the mean flow Mach number as established in Eq. (35)], the vorticity amplitude must be related to the pressure by

$$\omega' = -\frac{1}{M_b}\frac{\partial p'}{\partial z} + \mathbb{O}(M_b) = -\frac{k_m}{M_b}\sin(k_m z) + \mathbb{O}(M_b) \quad (39)$$

where the pressure gradient for the axial plane wave [from Eq. (29)] has been inserted. This is the unsteady consequence of the Crocco–Vazsonyi theorem. Notice that the required vorticity amplitude at the surface is several orders of magnitude higher than that implied in solutions [see arguments leading to Eq. (37)] that do not properly account for the no-slip boundary condition. The characteristic ratio M_b/k_m (or its inverse), that sets the magnitude of the vorticity, will play a central role in the time-dependent solution as it develops.

To summarize, a straightforward solution, based on simple longitudinal plane wave acoustic motion, suggests that the unsteady vorticity amplitude is of order M_b, and hence, negligible in combustion stability computations. However, application of correct boundary conditions indicates that vorticity must have a much larger value (on the order of k_m/M_b) if the no-slip condition is imposed. Therefore, one must endeavor to solve the complete unsteady problem to establish the effects of vorticity on motor stability.

IV. Unsteady Vorticity Effects

The results of the last subsection make it clear that vorticity effects must be accounted for even if the flowfield is assumed to be inviscid (as it is in the standard approach to combustion stability).[1-8] Viscous effects are usually incorporated by means of "acoustic boundary layer" theory, as for instance, in correcting for friction losses on inert surfaces.[14]

Earlier work,[13] aimed at correcting for vorticity produced at burning surfaces, followed a similar boundary-layer approach by assuming the flow to be dominated by viscous forces in a region of nonuniformity near the burning surface. The viscous region was assumed to be thin compared to the chamber radius because of the large acoustic Reynolds number. A simplified model of the mean flow could then be employed in the boundary region. Solutions were therefore valid only near the propellant surface leading other investigators to question their applicability in stability computations.[14]

The approach to be followed here is to avoid all such boundary-layer simplifications. A complete inviscid solution is carried out first. This will both simplify the analysis and emphasize the important fact that viscous forces are not required to account for production and transport of vorticity throughout the motor chamber. Effects of viscosity will then be recovered in a later section with the aim of handling problems involving high-frequency oscillations. Conditions under which viscous effects are important will be identified.

A. Calculation of the Unsteady Vorticity

The equation for vorticity is found by taking the curl of the momentum equation, Eq. (18). Thus,

$$ik\omega' = -M_b\nabla \times (u' \times \Omega + U \times \omega') \quad (40)$$

For an axially symmetric flow, only the azimuthal component is needed. It is governed by

$$ik_m\omega' - M_b \frac{\partial}{\partial r}(U_r\omega') - M_b \frac{\partial}{\partial z}(U_z\omega')$$

$$= M_b \left[\frac{\partial}{\partial r}(\Omega u') + \frac{\partial}{\partial z}(\Omega w')\right] \tag{41}$$

where ω' is the vorticity amplitude. Later manipulations are simplified by employing the transformation

$$\omega' = r\zeta' \tag{42}$$

Use of the continuity equation, Eq. (3), simplifies the mean flow terms. Dividing by U_r, one finds

$$-M_b \frac{\partial\zeta'}{\partial r} + i\frac{k_m}{U_r}\zeta' - M_b \frac{U_z}{U_r}\frac{\partial\zeta'}{\partial z}$$

$$= M_b \left[\frac{1}{rU_r}\frac{\partial}{\partial r}(\Omega u') + \frac{\partial}{\partial z}\left(\frac{\Omega}{rU_r}w'\right)\right] \tag{43}$$

Application of a simple perturbation approach to this equation by expanding in powers of the (small) mean flow Mach number does not work. Note that the highest-order derivative of ζ' is multiplied by the small parameter M_b. Neglect of this term as compared to the first-order terms would make it impossible to satisfy the boundary condition given in Eq. (39). It is necessary that the derivative with respect to r be retained to make available the necessary flexibility in the solution. This is a clear signal of a singular perturbation situation.[34,35]

The failure of a simple perturbation approach to the solution of Eq. (41) is a consequence of the presence of two length scales inherent in the problem. These are 1) the chamber radius R (used as the main scaling length), and 2) a length proportional to the radial distance traveled by a gas particle leaving the combustion zone in, e.g., one cycle of oscillation. The ratio of these lengths is proportional to the parameter M_b/k_m identified in earlier discussions as a key combination of variables. The significance here is that the presence of two length scales indicates the need, as in conventional boundary-layer analysis, to apply a singular perturbation approach. The small characteristic ratio M_b/k_m occurs so often in the analysis that it is appropriate to assign it a name. Put

$$\lambda = M_b/k_m \tag{44}$$

which lies in the range $0 < \lambda < 0.1$, for any solid propellant rocket system or cold flow simulation regardless of the mode of oscillation. The largest value in the inequality corresponds to a very long chamber (very low frequency) with an unusually high surface Mach number. Table 1 is a tabulation of properties for a variety of typical systems covering a wide range of key parameters. A typical small motor is represented by the sample introduced by Yang and Culick.[14] The large shuttle solid rocket motor (SRM) is at the opposite end of the spectrum. The cold-flow case[16] is included since it will be of interest to compare the flowfield predictions to experimental velocity distributions.

Since λ is small, powers of λ can be used to form a convenient perturbation sequence. Following the usual procedure, the radial variable is "stretched" so that retention of the highest-order derivative in a perturbation expansion of Eq. (43) can be justified. The form of Eq. (43) suggests that an appropriate radial variable is

$$\xi = (1 - r)/\lambda \tag{45}$$

and the corresponding perturbation expansion (usually called an "inner" expansion[34]) is

$$\zeta'(\xi, z, \lambda) + \zeta_0'(\xi, z) + \lambda\zeta_1'(\xi, z) + \lambda^2\zeta_2'(\xi, z) + \cdots \tag{46}$$

Using Eq. (45), one then finds that vorticity is governed by the perturbed first-order wave equation

$$\frac{\partial\zeta'}{\partial\xi} + i\frac{1}{U_r}\zeta' - \lambda\frac{U_z}{U_r}\frac{\partial\zeta'}{\partial z}$$

$$= \lambda\left[\frac{1}{rU_r}\frac{\partial}{\partial r}(\Omega u') + \frac{\partial}{\partial z}\left(\frac{\Omega}{rU_r}w'\right)\right] \tag{47}$$

The third term on the left may appear to be incorrectly placed. However, since the extent of the region in which vorticity effects dominate (a boundary layer is not assumed) has yet to be established, assumptions that would limit the range of validity must be avoided. The third term is retained since the ratio, $U_z/U_r = -\pi z r \cot(\frac{1}{2}\pi r^2) = -\pi z(1 - \lambda\xi)\tan(\pi\lambda\xi)$, grows rapidly from a zero value at the injection surface ($\xi = 0$) as radial position ξ increases. That is, $U_z/U_r = \mathcal{O}(\lambda^{-1})$ over a substantial volume of the chamber. Unless the motion is confined to vicinity of the surface, then the third term may be as important as the first two.

Expanding Eq. (47) by means of the series of Eq. (46), one finds that the first-order solution for the vorticity expansion must satisfy the boundary value problem:

$$\frac{\partial\zeta_0'}{\partial\xi} + \frac{i}{U_r}\zeta_0' - \lambda\frac{U_z}{U_r}\frac{\partial\zeta_0'}{\partial z} = 0 \tag{48}$$

$$\zeta_0'(0, z) = \lambda^{-1}\sin(k_m z) \tag{49}$$

The boundary condition, Eq. (49), is found by a similar expansion of Eq. (39). This linear first-order wave equation is readily solved by application of standard techniques. Note that the third term in Eq. (48)

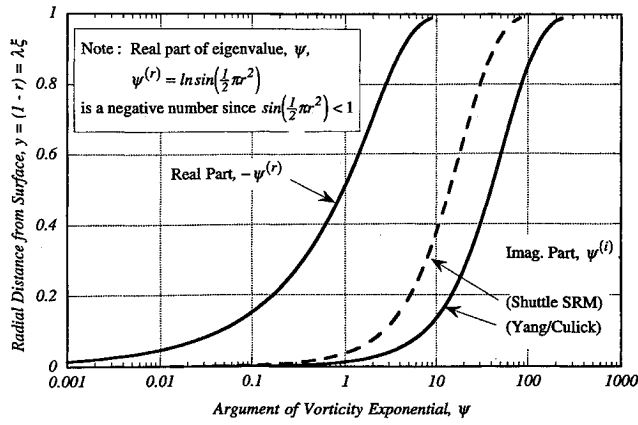$$\frac{U_z}{U_r} = -\frac{\pi r}{\tan(\frac{1}{2}\pi r^2)}z \tag{50}$$

involves the axial coordinate z. The sinusoidal term involving axial position in Eq. (49) must be therefore expanded in powers of z to allow matching with the boundary conditions. The usual power series is

$$\sin(k_m z) = k_m z - \frac{(k_m z)^3}{3!} + \frac{(k_m z)^5}{5!}$$

$$+ \cdots = k_m z \sum_{j=0}^{\infty} \frac{[-(k_m z)^2]^j}{(2j + 1)!} \tag{51}$$

Table 1 Physical parameters for typical motor systems

	L, m	R, m	L/D	M_b	k_1[a]	$\lambda = M_b/k_m$
Small research motor[14]	0.60	0.025	12.0	0.0017	0.133	0.0130
Tactical rocket, typical geometry	2.03	0.102	10.0	0.0030	0.157	0.0191
Cold flow experiment[16]	1.73	0.051	17.0	0.0033	0.093	0.0353
Space Shuttle SRM	35.10	0.700	25.0	0.0023	0.063	0.0367

[a]k_1 is the wave number for the first longitudinal mode, $m = 1$, where $k_m = m\pi R/L$.

Fig. 1   Real and imaginary parts of ψ.

Fig. 2   Function $\chi(r, z)$ vs axial position for several values of radius r.

Fig. 3   Vorticity amplitude vs y for several axial locations.

An appropriate characteristic solution for Eq. (48) is

$$(\zeta_0')_j = C_j(k_m z)^{2j-1} \exp[\psi_j(\xi)] \qquad j = 1, 2, 3, \ldots \quad (52)$$

where the corresponding eigenvalue is found by integrating

$$\frac{d\psi_j}{d\xi} = -\frac{i}{U_r} + (2j - 1)\lambda \left(\frac{U_z}{zU_r}\right) \quad (53)$$

Using the expression for the mean velocity components [Eq. (7)], one finds

$$\psi_j = (2j - 1)\psi^{(r)} + i\psi^{(i)} = (2j - 1)\pi \int \frac{r \, dr}{\tan(\frac{1}{2}\pi r^2)}$$

$$- \frac{i}{\lambda} \int \frac{r \, dr}{\sin(\frac{1}{2}\pi r^2)} \quad (54)$$

where real and imaginary parts of $\psi = \psi^{(r)} + i\psi^{(i)}$ are

$$\psi^{(r)} = l_n \sin(\frac{1}{2}\pi r^2) \quad (55)$$

$$\psi^{(i)} = -\frac{1}{\pi\lambda} l_n \tan(\frac{1}{4}\pi r^2) \quad (56)$$

At the surface ($r = 1, \xi = 0$), both real and imaginary parts vanish as indicated in Fig. 1. $\psi^{(r)}$ and $\psi^{(i)}$ vs radial position are shown for values of the parameter $\lambda = M_b/k_m$ covering a wide range of cases.

In order to satisfy the boundary condition, it is necessary to employ an infinite series of the eigenfunctions, $(\zeta_0')_j$. This allows the undetermined constants C_j to be found by means of Eq. (51). The result is

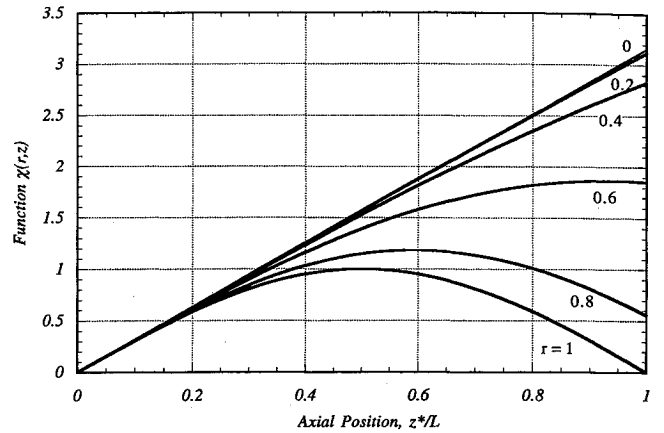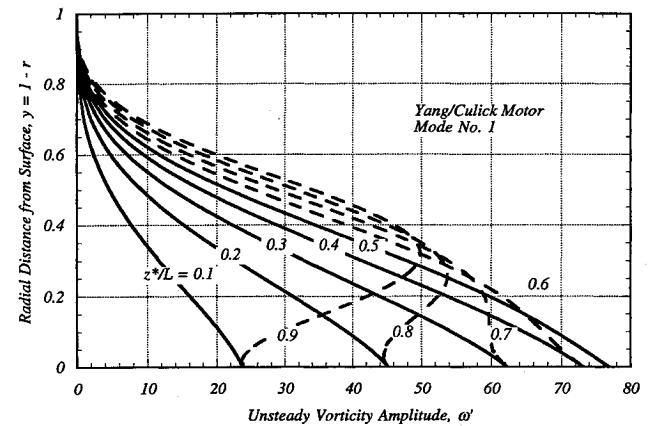$$C_j = \frac{(-1)^{j-1}}{\lambda(2j - 1)!} \quad (57)$$

Remembering that $\omega' = r\zeta'$, vorticity can finally be expressed as

$$\omega' = (r/\lambda)\exp(\psi)\chi(r, z) \quad (58)$$

where

$$\chi(r, z) = k_m z \sum_{j=0}^{\infty} \frac{(-1)^j(k_m z)^{2j}}{(2j + 1)!} \sin(\frac{1}{2}\pi r^2)^{2j} \quad (59)$$

The series solution converges rapidly and presents no particular computational problems. Notice that the influence of radial position remaining in the series involves only powers of the quantity $\sin(\frac{1}{2}\pi r^2)$, which has no effect near the burning

surface [since $\sin(\frac{1}{2}\pi r^2) = 1$ at $r = 1$]. Therefore, to very good approximation, one can simplify the solution to the useful form

$$\omega' = (r/\lambda)\exp(\psi)\sin(k_m z) = (r/\lambda)\sin(\frac{1}{2}\pi r^2)$$

$$\times \{\cos[\psi^{(i)}] + i \sin[\psi^{(i)}]\}\sin(k_m z) \quad (60)$$

valid near the injection boundary and in the forward end of the chamber. Corrections arising from the nonhomogeneous terms on the right of Eq. (47) are of order of the mean Mach number and can be safely neglected; they are several orders of magnitude smaller than the terms retained. The analytical results given here have been verified by comparison to solutions found by direct numerical integration of the complete problem.[19]

Equations (58) and (59) show that the vorticity varies as $\sin(k_m z)$ at the surface and becomes directly proportional to z near the chamber axis. Figure 2 is a plot of the axial dependence $\chi(r, z)$ for several radial positions. Figure 3 illustrates the solution for the vorticity for a typical case. Notice that the simplified solution given in Eq. (60) is valid anywhere in the forward part of the chamber $z^*/L < 0.3$, as Fig. 2 indicates. Axial position is expressed here as a fraction of the chamber length for convenience. The effects of the radial dependence in function $\chi(r, z)$ become more pronounced as z increases and the nozzle-end of the chamber is approached.

The solution indicates that vorticity is created by the action of the unsteady axial acoustic pressure gradient at the surface on the incoming mean flow as the boundary condition Eq. (39) shows. Equation (56) indicates that the wavelength of the oscillations is position-dependent (dispersive wave sys-

tem) and is controlled by the ratio $\lambda = M_b/k_m$. Either high-frequency oscillations or a very small injection Mach number leads to shorter spatial wavelength of the vortical waves. Hence, for very small values of λ (larger shearing stresses), rapid changes in particle direction may require retention of the viscous terms. This will be accomplished in Sec. VI.

B. Velocity Fluctuations with Inviscid Vortical Corrections

As already shown, the velocity fluctuations must have both irrotational and rotational parts. Hence, the velocity vector amplitude is written as the sum

$$u' = \hat{u} + \nabla \times S \tag{61}$$

where $\hat{u}$ is the acoustic (compressible, irrotational) part, and S is a vector potential that represents the solenoidal (incompressible, rotational) part of the motion. Thus, the part of the velocity field resulting from the production of vorticity is

$$\tilde{u} = \nabla \times S \tag{62}$$

where $S = Se_\theta$ if the flow is assumed axisymmetric for simplicity. Then the magnitude of the vector potential S is equivalent to the stream function (divided by r), and the composite velocity vector is

$$u' = \left(\hat{u} - \frac{\partial S}{\partial z}\right) e_r + \left[\hat{w} + \frac{1}{r}\frac{\partial}{\partial r}(rS)\right] e_z \tag{63}$$

where the acoustic solutions have already been described. The governing equation for S is found in terms of the vorticity by inserting Eq. (61) into Eq. (36) with the result

$$\nabla \times (\nabla \times S) = \omega' \tag{64}$$

Assuming axial symmetry and inserting the expression for vorticity from Eq. (59) yields

$$\frac{\partial^2 S}{\partial r^2} + \frac{1}{r}\frac{\partial S}{\partial r} - \frac{S}{r^2} + \frac{\partial^2 S}{\partial z^2} = -\omega' = -\frac{k_m}{M_b} r \exp(\psi)\chi \tag{65}$$

Only the particular solution is relevant; complementary solutions (involving modified Bessel functions of the first kind) are either singular or violate the zero radial velocity requirement at the chamber axis $(r = 0)$. The solution for the vector potential S, correct to first-order in λ, is

$$S = \lambda r U_r^2 \exp(\psi)\chi + \mathcal{O}(\lambda^2) \tag{66}$$

Using this result and Eq. (62) for the irrotational part, the velocity components are

$$u' = \hat{u} - \lambda r U_r^2 \exp(\psi)\frac{\partial \chi}{\partial z} + \mathcal{O}(\lambda^2) \tag{67}$$

$$w' = \hat{w} + ir U_r \exp(\psi)\chi + \mathcal{O}(\lambda) \tag{68}$$

where the expression for the radial acoustic velocity given by Eq. (34) and the axial acoustic velocity from Eq. (30) can be used in constructing the composite time-dependent velocity for a cylindrical chamber. Terms of order λ and higher are not displayed in the expressions for S and the axial velocity, since they are not needed in the stability calculations. Higher-order corrections are readily found if required. Notice that the axial velocity automatically satisfies the no-slip requirement since the equivalent boundary condition has already been applied to the vorticity.

Figures 4 and 5 show the amplitude of the axial velocity vs radius r for the forward and aft parts of the shuttle SRM motor chamber for several axial locations. The description of
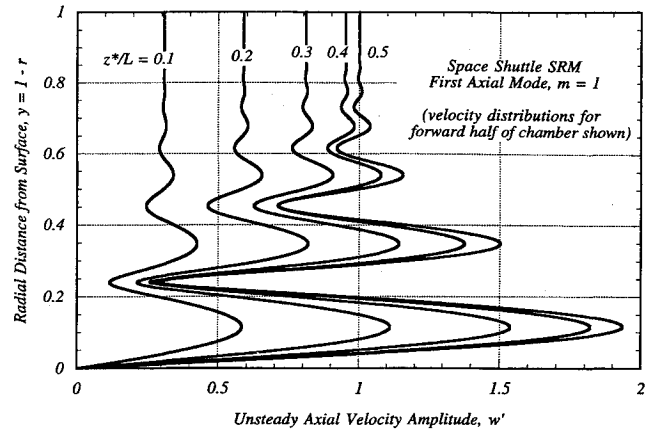

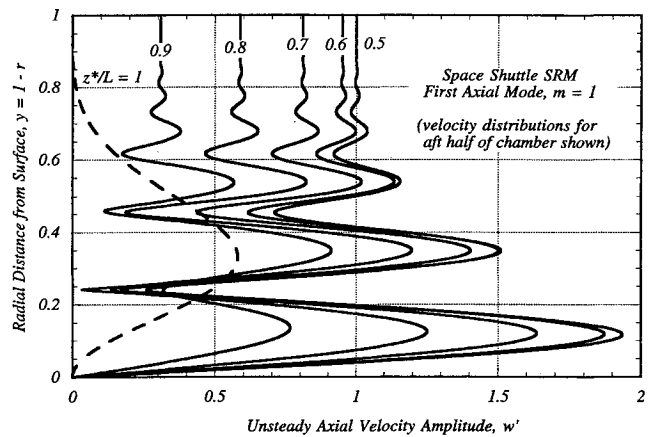Fig. 4 Axial velocity vs y for several axial locations in the forward half of the chamber.

Fig. 5 Axial velocity vs y for several axial locations in the aft half of the chamber.

the motion as a "vorticity wave" or shear wave suggested by Flandro[13] seems appropriate. The two halves are plotted separately to emphasize the unsymmetrical axial distribution arising from function χ. The shuttle example is used since, because of its low first-mode frequency (approximately 16 Hz for the fundamental axial mode), the spatial wavelength of the vorticity waves is a substantial fraction of the chamber radius. Only about three oscillation periods appear, making the graphs easier to interpret. Notice that the vortical velocity corrections die out radially even though there is no viscous dissipation represented. This is caused by the dependence on the radius r and the radial mean flow velocity U_r, which rapidly die to zero as the axis is approached. An interesting feature appears in the aft chamber plots. At the nozzle entrance, the axial vortical velocity component does not vanish as the acoustics part $[\hat{w} = i \sin(k_m z) = 0$ at $z = L/R]$ does. This is because the vorticity fluctuations are not compressibility waves; the rotational velocity corrections are solenoidal. That is,

$$\nabla \cdot \tilde{u} = \nabla \cdot \nabla \times S \equiv 0 \tag{69}$$

as readily seen from the definition of Eq. (62).

The usual nozzle boundary condition (using the nozzle admittance function, etc.) applies only to the acoustic (compressible) part of the oscillating flowfield. It does not account for the vorticity wave. Therefore, there may be an additional loss (or gain) of system energy represented by the flux of vibrational energy carried by the vortical motions across the nozzle boundary. At first glance, the dashed curve in Fig. 5 representing the vortical axial velocity at the nozzle entrance implies a quite large net flow of system energy compared to

the acoustical part (which is of order M_b). However, it is necessary to consider the vortical phase angle distribution across the nozzle entrance. Figure 6 shows the distribution of the real and imaginary parts of the vortical axial velocity fluctuation at the chamber aft boundary. The periodic variation shows that a surface integration of the real part of the vortical velocity across the nozzle will yield a small net energy flux. This and other new contributions to system stability will be evaluated in detail in the next section of this article.

The composite (acoustical + vortical) radial velocity is shown in Figs. 7 and 8 for the shuttle SRM at several axial locations
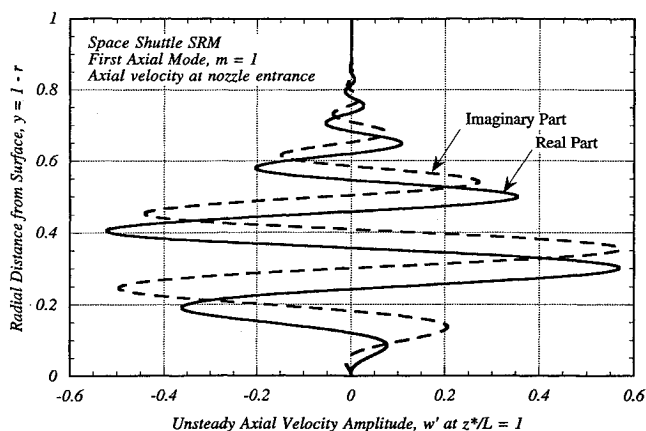

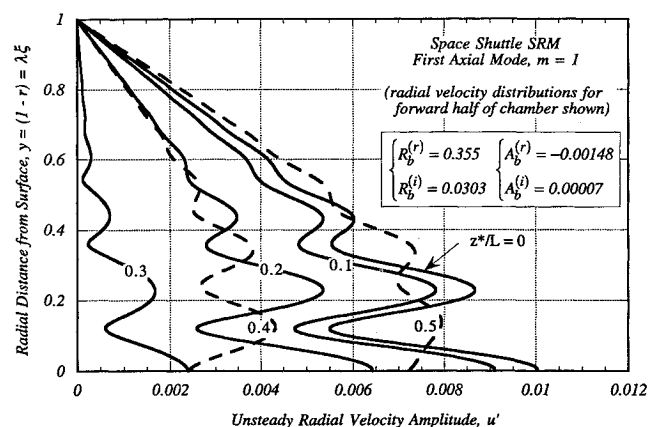**Fig. 6** Real and imaginary parts of the axial velocity vs y at the nozzle entrance.

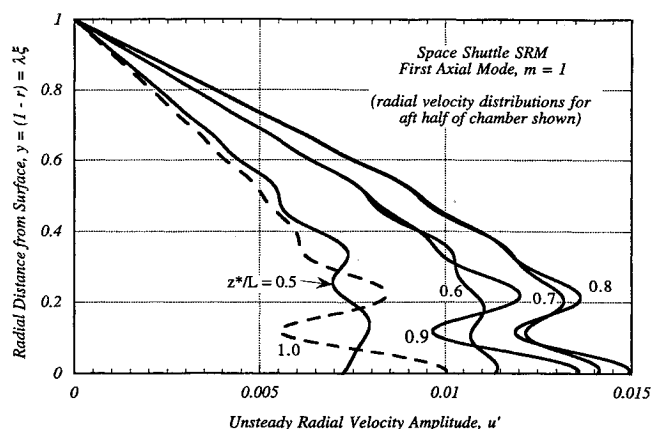**Fig. 7** Composite radial velocity vs y for forward half of chamber.

Fig. 8 Composite radial velocity vs y for aft half of chamber.

in the forward and aft sections of the motor chamber. The typical values of the propellant response function

$$R_b = (A_b + M_b)/M_b \tag{70}$$

shown on the graph were used in the expressions for the radial velocity, Eq. (67), since reliable measured values for the shuttle propellant at this low frequency (approximately 16 Hz) were not available.

C. New Normal Velocity Fluctuations at the Burning Surface— Mass Balance Considerations

Of considerable significance is the appearance of two new terms in the radial velocity that do not vanish at the boundary: 1) a correction from the vorticity production, Eq. (67), and 2) the new acoustic term proportional to the axial acoustic velocity, Eq. (35). These could very well represent part of the answer to Culick's implied question: ". . . something is evidently missing" expressed in his three-dimensional combustion stability analysis.[8] These new terms have the same significance as the admittance parameter itself in the surface coupling, since A_b is also proportional to the mean Mach number. They have not appeared in previous analyses for three reasons: 1) neglect of vorticity effects, 2) loss of the no-slip requirement in the three-dimensional analysis, and 3) neglect of the $\mathcal{O}(M_b)$ acoustic corrections.

Evaluating the expressions for the unsteady velocity components at the burning surface, one finds

$$u'(1, z) = -A_b \cos(k_m z) - M_b \cos(k_m z)$$
$$+ 2M_b R_v k_m z \sin(k_m z) \tag{71}$$

$$w'(1, z) = 0 \tag{72}$$

The second term in Eq. (71) that is proportional to the pressure fluctuation $p'_m = \cos(k_m z)$ is the new rotational flow correction. The rotational radial velocity series, $d\chi/dz$ in Eq. (67) collapses to the Taylor series for $\cos(k_m z)$. The vortical correction thus introduces a term that varies with location on the burning surface in the same manner as the pressure, and can thus be interpreted as an "admittance correction" as suggested earlier by Flandro.[13] However, the effect found here is an additional source of acoustic energy, since it increases the real part of the admittance. It is always negative (inward radial velocity), and depends on the pressure amplitude in the same manner as the pressure-coupled radial velocity. It is identical in form to the well-known mean flow driving effect that appears in the classical stability integrals (to be reviewed shortly), but it arises from an entirely different source, namely the rotational flow axial momentum defect at the propellant surface. This source is analogous to the radial flow generated in a simple steady flat plate boundary layer by the displacement effect.[36]

In the latter regard, reviewers of an early manuscript of this article expressed concern that terms like the two new ones appearing in Eq. (71) represent a violation of mass conservation. On the contrary, they must be present if continuity is to be satisfied. These conceptual difficulties arise because of the universal application of the simple acoustic admittance boundary condition to represent the gas motion at the edge of the burning zone. It must be pointed out that the admittance concept is based on an extension of acoustics methods that were not intended for application to boundaries with transpiration. The creation of mass at the burning surface requires the supplementary terms appearing in Eq. (71).

It is quite simple to show this directly from the continuity equation. For example, Eq. (69), the continuity equation for the rotational flow, can be used to solve directly for the radial velocity if the expression given in Eq. (68) for the axial velocity is inserted. Two constants of integration arising in the

solution of Eq. (69) are each zero in order that the radial velocity is not singular at the chamber axis.

The second new term is reminiscent of classical velocity coupling. However, it arises from the interaction of the axial pressure gradient with combustion in the presence of the mean flow vorticity. [Note z can be replaced by (Ω/π^2) at the surface from Eq. (12).] It is the outcome of the careful extension of the irrotational equations [see Eqs. (20) and (21) and subsequent discussions] to first-order in the mean flow Mach number; it has nothing to do with unsteady vorticity production. The stability implications of these new surface terms and other vortical corrections are the subject of the next section.

V. Effects of Unsteady Vorticity on System Stability

It is now possible to assess the effects of a realistic unsteady rotational flowfield solution on the system stability. Since new stability terms are involved, a complete treatment of the stability problem is presented to assist those not familiar with previous efforts. The steps are similar in most respects to the methods applied by Culick in his assessment of acoustic (irrotational) stability properties of solid propellant motors.[3,5,7,8] What follows is a preliminary discussion of a very complicated subject. The object of the calculations is to estimate the growth rate of the combined acoustic/rotational wave system. A benefit of this method is that the various contributing stability integrals are additive due to mathematical linearity. This allows a careful assessment of each new gain or loss term and its relative effect on motor stability.

A. Stability Calculations

The system stability is governed by the perturbed Helmholtz equation and a corresponding perturbed boundary condition on pressure gradient at the chamber boundaries. These equations are found by using Eqs. (17) and (18) in the manner described in Culick's papers.[3,5,7,8,14] One finds

$$\nabla^2 p' + k^2 p' = -ikM_b U \cdot \nabla p' - M_b \nabla \cdot [\nabla(u' \cdot U)$$
$$- u' \times \Omega - U \times \omega'] \quad (73)$$

$$n \cdot \nabla p' = ikn \cdot u' - M_b n \cdot (\nabla u' \cdot U$$
$$- u' \times \Omega - U \times \omega') - \delta^2 n \cdot \nabla \times \omega' \quad (74)$$

where all terms involving the vorticity (including the viscous force term) are now correctly represented. Pressure is chosen as the principal variable, since it is the parameter measured in most experiments. Following Culick's notation, put

$$\nabla^2 p' + k^2 p' = h \quad (75)$$

$$n \cdot \nabla p' = -f \quad (76)$$

where

$$h = -ikM_b U \cdot \nabla p' - M_b \nabla \cdot [\nabla(u' \cdot U)$$
$$- u' \times \Omega - U \times \omega'] \quad (77)$$

$$f = -ikn \cdot u' + M_b n \cdot (\nabla u' \cdot U - u' \times \Omega$$
$$- U \times \omega') + \delta^2 n \cdot \nabla \times \omega' \quad (78)$$

In earlier studies the first term in function f would now be replaced by an equivalent admittance function. This will not be done here, because as shown in the last subsection, there are other contributions to the normal velocity fluctuation that are not represented by the acoustic admittance function alone.

The simplest approach to extracting the necessary stability properties is to represent the system motion as a perturbation around a known unperturbed solution, namely one of the normal acoustic modes of the chamber. Therefore, the per-

turbed solution can be written in terms of an infinite series of the chamber acoustic eigenfunctions as

$$p' = \sum_{i=1}^{\infty} A_i p'_i = p'_m + \sum_{\substack{i=1 \\ i \neq m}}^{\infty} A_i p'_i = p'_m + \mathcal{O}(M_b) \quad (79)$$

where p'_m is the mode of oscillation whose stability is to be estimated. p'_m is a solution of the set

$$\nabla^2 p'_m + k_m^2 p'_m = 0 \quad (80)$$

$$n \cdot \nabla p'_m = 0 \quad (81)$$

The evaluations carried out in what follows utilize the simple axial plane wave solutions [see Eqs. (29) and (30)], but the same method applies to any acoustic mode. In general, m represents a set of up to three mode integers to represent a complex combined mode consisting of transverse as well as axial oscillations. In the present case m is a single integer; $m = 1$ represents the fundamental longitudinal acoustic mode.

As discussed earlier [see Eq. (16)] the perturbed wave number can be written as

$$k = k_m + M_b k_\alpha = k_m + (\omega_m + i\alpha_m) + \mathcal{O}(M_b^2) \quad (82)$$

where k_m is the acoustic wave number corresponding to mode m under investigation. The complex correction to the wave number contains $\mathcal{O}(M_b)$ terms that represent the shift in oscillation frequency due to the perturbations and the important quantity α_m that represents the growth rate of the system. The object of the following analysis is to estimate the growth rate. Positive values of α_m indicate an unstable mode m, etc., as in previous studies. After application of several vector identities and integral theorems, one finds

$$\omega_m = \frac{1}{2k_m E_m^2} \mathfrak{R} \left(\int\int_V\int hp'_m \, dV + \int\int_S fp'_m \, dS \right) \quad (83)$$

$$\alpha_m = \frac{1}{2k_m E_m^2} \mathfrak{I} \left(\int\int_V\int hp'_m \, dV + \int\int_S fp'_m \, dS \right) \quad (84)$$

This result is identical to that forming the basis of the existing standard stability algorithms except that new terms now appear in both functions h and f. The integrals containing these new terms must be carefully evaluated to determine the effects of vorticity on system stability. Also, the surface conditions in f must reflect the correct normal velocity fluctuation as given in Eq. (71).

The integrals can be simplified by application of Green's theorem and standard vector identities. The steps are identical to those described in earlier works and need not be repeated here. For the growth rate one finds

$$\alpha_m = \frac{1}{2E_m^2} \mathfrak{I} \left[\begin{array}{c} -iM_b \int\int_S \left(\frac{1}{M_b} n \cdot u' p'_m + n \cdot U p'^2_m\right) dS \\ -\frac{\delta^2}{k_m} \int\int_S \frac{\partial \omega'}{\partial z} p'_m \, dS \\ + k_m M_b \int\int_V\int (\bar{u} \cdot U) p'_m \, dV \\ -\frac{M_b}{k_m} \int\int_V\int (U \times \omega') \cdot \nabla p'_m \, dV \end{array} \right] \quad (85)$$

A similar expression, involving the real parts of the integrals, gives the frequency correction. This expression must be multiplied by the inverse of the characteristic time R/α_0 to convert

Table 2 Summary of stability integrals with rotational flow corrections[a]

Symbol[b]	Description	General three-dimensional integral	
$\hat{\alpha}_{C_1}$	Classic pressure coupling with mean flow effect (~ response function)	$\dfrac{1}{2E_m^2}\left(\dfrac{a_0}{R}\right)\displaystyle\int_{S_b}\int [A_b^{(r)} + M_b]p_m'^2\,dS$	(88)
$\tilde{\alpha}_{C_2}$	Rotational flow correction due to induced radial velocity	$\dfrac{1}{2E_m^2}\left(\dfrac{a_0}{R}\right)\displaystyle\int_{S_b}\int M_b p_m'^2\,dS$	(89)
$\hat{\alpha}_{N_1}$	Classical nozzle damping	$-\dfrac{1}{2E_m^2}\left(\dfrac{a_0}{R}\right)\displaystyle\int_{S_N}\int [A_N^{(r)} + M_b U_z]p_m'^2\,dS$	(90)
$\tilde{\alpha}_{N_2}$	Additional nozzle damping due to rotational axial flow component	$-\dfrac{1}{2E_m^2}\left(\dfrac{a_0}{R}\right)\Re\displaystyle\int_{S_N}\int (e_z\cdot\bar{u})p_m'\,dS$	(91)
$\hat{\alpha}_{VC_1}$	Classical velocity coupling	Not defined in present analysis	
$\hat{\alpha}_{VC_2}$	Correction to normal surface velocity (similar to velocity coupling)	$\dfrac{M_b}{\pi^2 E_m^2}\left(\dfrac{a_0}{R}\right)R_v^{(r)}\displaystyle\int_{S_b}\int \Omega_{surface}p_m'\frac{dp_m'}{dz}\,dS$	(92)
$\tilde{\alpha}_{FT}$	Three-dimensional form of flow-turning loss	$-\dfrac{1}{2E_m^2}\left(\dfrac{a_0}{R}\dfrac{M_b}{k_m}\right)\oint\int_V\int (U\times\omega')\cdot\nabla p_m'$	(93)
$\tilde{\alpha}_{V_1}$	Interaction of mean flow and rotational velocity fluctuation	$\dfrac{k_m M_b}{2E_m^2}\left(\dfrac{a_0}{R}\right)\oint\int_V\int (\bar{u}\cdot U)p_m'\,dV$	(94)
$\tilde{\alpha}_{FD}$	Direct viscous damping effect	$-\dfrac{1}{2E_m^2}\left(\dfrac{a_0}{R}\right)\dfrac{\delta^2}{k_m}\oint\int_S\int \frac{\partial\omega'}{\partial z}p_m'\,dS$	(95)

[a]Results tabulated are growth rates in dimensional form (s⁻¹). Particle damping not shown.
[b]Caret mark ($\hat{\alpha}$) identifies terms of acoustic origin; tilde ($\tilde{\alpha}$) represents terms of vortical origin.

the result to dimensional form to aid in comparisons with other solutions. The growth rate is usually expressed in the same units as the circular frequency (in rad/s or s⁻¹). For axial modes the normalization function (dimensionless) is

$$E_m^2 = \int\int_V\int \cos^2(k_m z)\,dV = \pi\left(\frac{L}{2R}\right) \quad (86)$$

As much of the integration as possible at this point has been reduced to surface integral form by application of Green's theorem. Further simplification can be accomplished only after the behavior of the volume integrals has been examined. Equation (85) does not display particulate damping terms or other established effects such as viscous losses at inert surfaces. Due to linearity, these can simply be added as needed. Also not shown is the influence of the terms in h and f proportional to $(u' \times \Omega)\cdot\nabla p_m'$. These lead to a negligible stability correction since $u' \times \Omega$ is nearly perpendicular to the pressure gradient vector $\nabla p_m'$ for longitudinal modes. Note that statements of the sort just made may only apply to the assumed axial mode problem considered here.

The system stability is most often represented as an additive series of stability integrals for each mode m

$$\alpha_m = \alpha_C + \alpha_{VC} + \alpha_N + \alpha_{FT} + \cdots \quad (87)$$

where the contributions of particulate damping α_p, viscous surface losses α_V, etc., have been evaluated elsewhere[1-5,14] and form the backbone of the existing stability algorithms. It has been the usual practice to represent α_{FT} by the flow-turning expression found in the one-dimensional analysis.[8] In what follows we will show that introduction of the vorticity corrections leads to an equivalent three-dimensional stability integral. Since several new terms arise as a result of relaxing the irrotational flow assumption, it is useful to modify the standard notation in Eq. (87) to better reflect the origin of each stability integral.

Table 2 introduces modified symbols and describes the physical origin of each term. Numerical subscripts are appended when a new term significantly modifies one of the classical ones with which it is closely connected. A caret mark ($\hat{\alpha}$) over a particular contribution indicates that it originates from acoustical effects; tilde ($\tilde{\alpha}$) is used as usual to denote terms that originate from rotational flow effects.

An important influence of the effect of vorticity transport is immediately apparent in Table 2. The rotational flow term $\tilde{\alpha}_{C_2}$ resulting from the radial velocity correction [see Eq. (71)] leads to the new growth rate increment shown in Eq. (89). If this term is combined with the classical combustion driving represented by $\hat{\alpha}_{C_1}$, it is apparent that the new term doubles the effect of the familiar flow-driving effect

$$-n\cdot M_b U = M_b \quad (96)$$

appearing in the surface integral of Eq. (88). It thus represents a significant destabilizing influence that does not appear in the standard irrotational stability analysis.

The classical nozzle damping is shown in Eq. (90). The combination $M_b U_z = M_N$ is equivalent to the Mach number at the nozzle entrance as usually written. Provision is made in Eq. (91) for the loss represented by flux of rotational wave energy through the nozzle, although, as already explained, this is small.

No provision is made here for classical velocity coupling since most models require a crossflow velocity at the burning surface. In the present analysis, the no-slip condition precludes a direct influence of the axial acoustic motion on the combustion processes. Nevertheless, as discussed in detail earlier, a new acoustic flow interaction term appears naturally that exhibits many of the characteristics associated with velocity coupling. Thus, as suggested in Table 2, this can be represented by the usual velocity coupling notation. Subscript 2 in Eq. (92) indicates that this is an addition to the classical effect. The caret mark indicates that it is of acoustic, not vortical, origin.

Table 3   Evaluation of stability integrals for cylindrical motor chambers

Growth rate increment	Cylindrical grain segment of length Δz located at position z	Full-length cylindrical chamber	
$\hat{\alpha}_{C_1}$	$\dfrac{a_0}{L}[A_b^{(r)} + M_b]\left\{\Delta z + \dfrac{\sin[2k_m(z + \Delta z)] - \sin(2k_m z)}{2k_m}\right\}$	$\dfrac{a_0}{R}[A_b^{(r)} + M_b]$	(97)
$\hat{\alpha}_{C_2}$	$\dfrac{M_b a_0}{L}\left\{\Delta z + \dfrac{\sin[2k_m(z + \Delta z)] - \sin(2k_m z)}{2k_m}\right\}$	$\dfrac{M_b a_0}{R}$	(98)
$\hat{\alpha}_{N_1}$	$-\dfrac{a_0 A_b^{(r)}}{L} - \dfrac{2M_b a_0}{L}\Delta z$	$-\dfrac{a_0 A_b^{(r)}}{L} - \dfrac{2M_b a_0}{R}$	(99)
$\hat{\alpha}_{N_1}$	Negligible correction	Negligible correction	
$\hat{\alpha}_{VC_2}$	$-\dfrac{M_b a_0 R_\nu^{(r)}}{L}\left\{\begin{array}{l}\dfrac{\sin[2k_m(z + \Delta z)] - \sin(2k_m z)}{2k_m}\\ -\Delta z\cos[2k_m(z + \Delta z)]\end{array}\right\}$	$\dfrac{M_b a_0 R_\nu^{(r)}}{R}$	(100)
$\hat{\alpha}_{FT}$	$-\dfrac{M_b a_0}{L}\left\{\Delta z - \dfrac{\sin[2k_m(z + \Delta z)] - \sin(2k_m z)}{2k_m}\right\}$	$-\dfrac{M_b a_0}{R}$	(101)
$\hat{\alpha}_{VI}$	$\mathcal{O}(M_b^2)$	$\mathcal{O}(M_b^2)$	
$\hat{\alpha}_{FD}$	Negligible correction	Negligible correction	

The volume integral in Eq. (93) is identified as the three-dimensional equivalent of the one-dimensional flow-turning effect. A detailed explanation for this result is given in the evaluations in the next subsection. Two other new effects related to rotational flow corrections appear in Eqs. (94) and (95). These will be shown to have negligible effect on growth or decay of the wave system.

Other stability integrals not shown here may be significantly modified by the rotational flow corrections. For instance the particulate damping is strongly affected because the particle drag depends on the details of the local gas motion. The major distortion of the acoustic mode shapes by the vorticity waves must be accounted for in these calculations. Correction of the particulate damping is the subject of another paper in preparation at the time of writing.

B.   Evaluation of Stability Integrals for Cylindrical Chambers

The results shown in Table 2 are quite general. For the most part they are applicable to any chamber geometry. It is instructive to evaluate the stability integrals for a simple, but realistic, motor geometry. This can be accomplished in closed form for cylindrical motor grains. Table 3 is a summary of such evaluations for the integrals described in Table 2. Both partial and full length grain segments are analyzed. The partial grain results can be superimposed to give stability information for multiple grain configurations such as an extended area T-burner or sonic end-vent burner.

For a cylindrical geometry, the surface integrations are carried out easily. The results for the acoustic parts are identical to those found in previous studies. The volume integrations require more explanation, because they involve spatial oscillations represented by factors such as $\exp[i\psi^{(i)}]$ arising in the rotational flow corrections. It is very difficult to carry out these integrations in closed form unless one takes advantage of certain features of the integrands.

To demonstrate the evaluation method, integration of the flow-turning expression in Eq. (93) will be described in detail. This is an important contribution to the system energy balance because the unsteady vorticity is of the order of the inverse of the mean flow Mach number rather than directly propor-

tional to M_b as assumed by previous investigators. The integrand consists of the product of a mean flow term changing slowly with radial position and the unsteady vorticity ω', which rapidly oscillates with radial position r. For a cylindrical chamber

$$U \times \omega' = (-U_z \omega')e_r + (U_r \omega')e_z \qquad (102)$$

and for a plane acoustic wave

$$\nabla p_j' = -k_m \sin(k_m z)e_z \qquad (103)$$

Therefore, the integrand in Eq. (93) is

$$(U \times \omega') \cdot \nabla p_m' = -k_m U_r \omega' \sin(k_m z) \qquad (104)$$

Using Eq. (58) for the vorticity and inserting Eq. (86) for E_m^2, one finds

$$\bar{\alpha}_{FT} = \left(\frac{2M_b a_0}{\lambda L}\right) \oint \int_0^{L/R} \int_0^1 r^2 U_r \sin(\tfrac{1}{2}\pi r^2)$$

$$\times \exp[i\psi^{(i)}]\chi(r, z)\sin(k_m z)\, dr\, dz \qquad (105)$$

The integrals are readily carried out numerically (fourth-order Runge–Kutta was used here); the results point the way to closed-form expressions. Figure 9 shows typical plots of the integrand and the corresponding integral for a given axial location. Notice that the integrand starts at zero at the lower limit and oscillates around zero all the way to the outer limit ($r = 1$). Therefore, the value of the integral depends only on its value at the surface. The integral at the upper limit can be easily evaluated because of numerous simplifications that apply when $r \approx 1$. For example, the radial mean flow can be replaced by $U_r = -1$, and $\sin(\tfrac{1}{2}\pi r^2) \to 1$. Of even greater value is the simplification of the exponential involving $\psi^{(i)}$. In the vicinity of $r = 1$, one can write

$$\psi^{(i)} = -(1/\pi\lambda)/_r \tan(\tfrac{1}{4}\pi r^2) \approx (1/\lambda)(1 - r) \qquad (106)$$
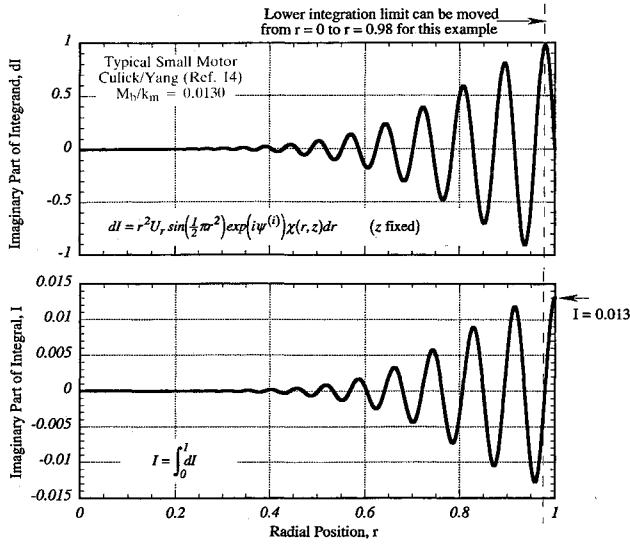
Fig. 9 Numerical behavior of radial integral of Eq. (105).

and as already shown, function χ has the limiting value

$$\chi(1, z) = k_m z \sum_{j=0}^{\infty} \frac{(-1)^j (k_m z)^{2j}}{(2j + 1)!} = \sin(k_m z) \quad (107)$$

near the burning surface. Therefore, the integral at the upper limit (and, hence, the entire value of the integral) gives

$$\bar{\alpha}_{FT} = -\frac{2M_b a_0}{\lambda L} \oint \left\{ \int \exp[i\psi^{(i)}] \, dr \right\}_{r=1} \int_{z_1}^{z_2} \sin^2 (k_m z) \, dz \quad (108)$$

where z_1 and z_2 denote the locations of the ends of a cylindrical grain segment.

Finally, the exponential integral is easily evaluated using Eq. (106) with the result

$$\int \exp[i\psi^{(i)}] \, dr = \exp\left(i \frac{k_m}{M_b}\right) \int \exp\left(-i \frac{k_m}{M_b} r\right) \, dr$$

$$= i \frac{M_b}{k_m} \exp\left(i \frac{k_m}{M_b}\right) \exp\left(-i \frac{k_m}{M_b} r\right)_{r=1} = i\lambda \quad (109)$$

and the flow-turning loss for a cylindrical grain of arbitrary length is

$$\bar{\alpha}_{FT} = -\frac{2M_b a_0}{L} \int_{z_1}^{z_2} \sin^2(k_m z) \, dz \quad (110)$$

The z integral is evaluated in Table 3 [Eq. (101)] for both a partial grain segment and a full-length cylindrical propellant grain. All other volume integrals involving vorticity wave effects are handled in the same manner.

Evaluation of surface integrals across transverse boundaries of the solution domain, such as the nozzle entrance plane, are also aided by the simplifications just discussed. For example, a similar analysis shows that the second nozzle term [Eq. (91)] is negligible because the integral is nearly zero at the surface. Examination of Fig. 6 in the light of the findings described in the last few paragraphs will verify this conclusion.

To apply the results shown in Table 3, it is only necessary to add the appropriate terms and insert the parameter values for the motor being evaluated. As a simple example, consider the shuttle SRM geometry. If one assumes a full length grain at midburn and neglects effects of vortex shedding, velocity

coupling, and other influences of the intersegment gaps, the net growth rate is

$$\alpha_m = (a_0/R)[A^{(r)}_{;i} - M_b] - (a_0/L)A^{(r)}_N \quad (111)$$

where several of the terms in Table 3 cancel. Notice that the sum of the flow-turning and the new surface term $\bar{\alpha}_{C_2}$ is zero. This cancellation only occurs for a full-length grain. Study of Table 3 shows that because of differences in z dependence such a cancellation does not occur in partial grains. If the standard quasisteady short nozzle result[14]

$$A^{(r)}_N = [(\gamma - 1)/2]M_N = (\gamma - 1)(L/R)M_b \quad (112)$$

is used in Eq. (111) with an estimated (measured values are not available) admittance function, the growth rate for the first mode is $\alpha_1 = -6.6 \text{ s}^{-1}$, which is somewhat larger than the values estimated by others. That is, the present analysis suggests that the shuttle motor is less stable than previous estimates indicate. This helps to explain the appearance of low-amplitude axial oscillations in the shuttle SRM driven, apparently, by vortex shedding at the segment interfaces.[29-31]

C. Reduction of the Flow-Turning Correction to a Surface Integral

It is useful to apply additional simplifications to the flow-turning term. It has already been shown that the value of the volume integral depends only on the behavior of the integrand near the injection surface at $r = 1$. This suggests that it may be possible to convert to surface integral form. This is readily accomplished if the vorticity is approximated in the integrand, Eq. (104), as

$$\omega' = \frac{\partial \bar{u}}{\partial z} - \frac{\partial \bar{w}}{\partial r} \approx -\frac{\partial \bar{w}}{\partial r} \quad (113)$$

This is valid since the radial velocity is very small and changes only slowly with axial position. Also, the integrand goes rapidly to zero at the centerline as already demonstrated (see Fig. 9). The value of the radial part of the volume integral is determined entirely by its upper limit at $(r = 1)$. The integrand can then be approximated by

$$(U \times \omega') \cdot \nabla p'_m = k_m U_r \frac{\partial \bar{w}}{\partial r} \sin(k_m z) \approx -\frac{\partial}{\partial r} (U_r \bar{u} \cdot \nabla p'_m) \quad (114)$$

since the vorticity (and, hence, the derivative of the velocity with respect to r) is proportional to $1/\lambda$. Therefore, the volume integral can be replaced by an equivalent surface integral giving

$$\alpha_{FT} = -\frac{M_b}{2k_m E_m^2} \left(\frac{a_0}{R}\right) \oint_{S_b} \int \bar{u} \cdot \nabla p'_m \, dS \quad (115)$$

where terms of higher order in M_b have not been displayed. The validity of this transformation to surface integral form has been verified by numerical evaluation of the radial part of Eq. (93). The new expression, Eq. (115), is also valid for a fully three-dimensional port geometry. Note that the integration is only to be taken over the lateral boundaries with incoming mass flux, since the original form was a volume integral. That is, it is inappropriate to integrate Eq. (115) over the transverse chamber boundaries.

The three-dimensional form for the flow-turning, Eq. (115), is preferable to the one-dimensional form since it more clearly displays the physical origin of this important stabilizing effect. The new expression is written in terms of the rotational part of the velocity fluctuation $\bar{u}$. Notice that α_{FT} vanishes if one assumes the flow is irrotational as is done in the current three-

dimensional version of the SSPP algorithm. Thus, "patching" the one-dimensional flow-turning is not a valid approach unless all such rotational flow corrections are incorporated. Since the no-slip condition is satisfied, the value of the axial component of $\bar{u}$ at the surface is equal and opposite to the value of the acoustic velocity $\hat{u}$, parallel to the surface in the absence of the vorticity corrections. Thus, evaluation of the three-dimensional flow-turning surface integral requires only knowledge of the acoustic mode pressure and velocity distributions, since $w' = \hat{w} + \bar{w} = 0 \rightarrow \bar{w} = -\hat{w}$ at the burning surface.

D. Comparison of the One- and Three-Dimensional Flow-Turning Results

Since the subject of flow-turning has been a controversial one for many years, it is appropriate to discuss briefly the new findings vis-à-vis the original loss term that arose in a one-dimensional stability analysis.[7,8] The first order of business is a demonstration that Eq. (115) is exactly equivalent to the one-dimensional result. For a plane acoustic wave, one finds for the integrand of Eq. (115) at the surface

$$\bar{u} \cdot \nabla p'_m = \bar{w} \frac{\partial p'_m}{\partial z} = \frac{i}{k_m} \left(\frac{\partial p'_m}{\partial z} \right)^2 \qquad (116)$$

Therefore,

$$\alpha_{\mathrm{FT}} = -\frac{M_b}{2k_m E_m^2} \left(\frac{a_0}{R} \right) \oint \int \int_S \bar{w} \frac{\partial p'_m}{\partial z} \, dS$$

$$= -\frac{M_b a_0}{\pi L} \int \int_S \frac{1}{k_m^2} \left(\frac{\partial p'_m}{\partial z} \right)^2 dS \qquad (117)$$

This is exactly equivalent to the one-dimensional formula given by Culick [see Eq. (4.1) in Ref. 8] using slightly different notation. It must be emphasized again that all terms of vortical origin must be included in the stability calculations. It is therefore not correct to append Eq. (117) to the original irrotational stability formulation without accounting for several other terms of equal importance as shown in Table 3.

VI. Viscous Corrections

The rotational combustion stability theory described in previous sections is based on an approximation, valid in a great many situations, that viscous effects are negligible. This may not be true for propellants with very low burning rate or for high-frequency acoustic modes because the shearing stresses might then lead to important viscous effects. The results of the inviscid theory makes it a simple matter to include the viscous forces, since, as demonstrated in the last subsection, the important flow interaction effects depend only on conditions near the burning surface. Hence, some of the ideas of acoustic boundary-layer theory are applicable. It is not necessary to deduce the complete viscous solution to find the necessary information.

The earlier acoustic boundary-layer results of Flandro[13] are now interpreted in light of the new information. In particular, the much criticized assumption used in that work that the mean flow velocity could be approximated by $U = -e_r$ is valid, since only the motion near the surface must be accurately represented. Effects of boundary curvature were also neglected, again on the basis that only the motion in a thin region at the burning surface required attention. Equations (5) and (6) were then expanded in the same manner used in this article, but with viscous terms retained. A stretched radial coordinate

$$\eta = y/\delta = (1 - r)/\delta \qquad (118)$$

was introduced based on the viscous characteristic length δ instead of λ, as used herein [see Eq. (45)]. Expressions for the velocity valid near the surface for an assumed longitudinal planar acoustic wave were then determined. The no-slip condition was satisfied, giving the unsteady velocity components

$$u' = -A_b \cos(k_m z) - \frac{i k_m \delta(a - ib)}{a^2 + b^2} e^{-(a+ib)\eta} \cos(k_m z) \qquad (119)$$

$$w' = i[1 - e^{-(a+ib)\eta}] \sin(k_m z) \qquad (120)$$

where u' is written here as the radial velocity (r direction is opposite to the y direction), and the sign on the axial velocity is reversed to reflect the different reference phase angle used in Ref. 13. The real and imaginary parts of the exponential terms involving η are found from

$$a^2 - b^2 + (M_b/\delta)a = 0 \qquad (121)$$

$$2ab + (M_b/\delta)b = k_m \qquad (122)$$

As much of the original notation as possible is retained consistent with the need for compatibility with the new inviscid analysis. Also, the nonisentropic corrections retained in the earlier analysis are dropped for consistency with the basic assumptions used here. The acoustic radial velocity created by the reactive wall condition has been added to Eq. (119) to avoid the need to define special admittance functions at the solid surface and at the edge of the vortical layer as used in Ref. 13. In fact, that approach is valid only if the motion is indeed of the boundary-layer type with the rotational effects confined to a region of about the same thickness as the burning zone. Again, as in the inviscid case, the motion consists of vorticity waves as evidenced by the complex exponential (damped sinusoidal) functions describing dependence on radial position. The real and imaginary parts of the radial eigenvalue from Eqs. (121) and (122) are

$$a = \tfrac{1}{2}[(k_m/b) - (M_b/\delta)] \qquad (123)$$

$$b = \sqrt{\tfrac{1}{8}\{-(M_b/\delta)^2 + \sqrt{(M_b/\delta)^4 + (4k_m)^2}\}} \qquad (124)$$

The motion is now controlled by three parameters rather than just two as in the inviscid case. Figure 10 shows plots of these expressions for an appropriate range of the variables. Use of Eq. (120) in evaluating the flow-turning loss in Eq. (115) leads to a result identical to that found in the last subsection. That is, flow-turning depends ultimately only on the requirement that the no-slip condition is met. Judgments, such as those in Ref. 14, that ". . . flow-turning losses are distinct from those associated with the acoustic boundary layer," and ". . . be-
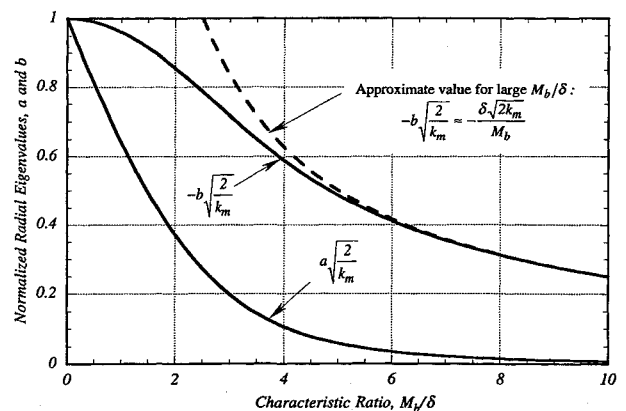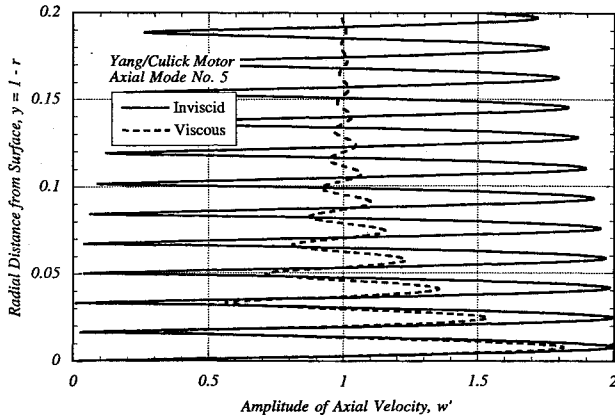

Fig. 10 Viscous flow eigenvalues.

Fig. 11 Effects of viscosity on vortical wave motion, fifth longitudinal mode ($m = 5$).

Fig. 12 Effects of viscosity on vorticity gain correction.

cause the flow far from the surface is in the perpendicular direction (in acoustic boundary-layer theory), there is no possibility of capturing the flow-turning effect" are, therefore, inaccurate.

Figure 11 compares the inviscid theory to the viscous results for the Yang/Culick motor. The Space Shuttle SRM case is not shown since the viscous and inviscid solutions are virtually identical near the surface. The plots represent the behavior of the axial velocity component near the burning surface for the fifth axial mode. Since this is a small motor with relatively high axial mode frequencies and moderate burning rate, it represents a case that is significantly affected by viscous forces for larger mode numbers. An important consequence of the viscous effects is the more rapid convergence to the plane wave geometry as distance y from the surface increases. Nevertheless, all important features of the motion are captured by the simplified inviscid theory. In particular, the slope of the velocity distribution near the surface and the locations of the first two peaks in the velocity amplitude are in close agreement. The slope is very nearly equal to the vorticity, showing that the viscous calculations yield the same surface vorticity as that found earlier [see discussions leading to Eq. (39)]. Therefore, any calculations, such as the flow-turning loss $\bar{\alpha}_{FT}$ or rotational flow gain $\bar{\alpha}_{C_2}$, requiring information concerning the oscillating velocity near the surface, are well-represented by either model. Again, only for very high-frequency oscillations and very low burning rate, is it necessary to incorporate the viscous corrections, but these do not alter the important stability integrals. The mathematical model displayed in this subsection gives an accurate assessment of the flow-turning and the new vortical gain effect for any case of practical interest. Thus, except for misinterpretation of the results, the earlier work given in Ref. 13 contains all essential elements needed for correct handling of the effects of vorticity on the three-dimensional combustion stability boundary conditions.

The viscous equivalent of the rotational flow gain effect $\bar{\alpha}_{C_2}$ can be readily deduced from Eq. (119). At the surface ($\eta = 0$), the radial velocity is

$$u' = -A_b \cos(kz) - \frac{k_m \delta(b + ia)}{a^2 + b^2} \cos(kz) \qquad (125)$$

and the viscous rotational flow gain correction can be calculated by analogy with the inviscid analysis that leads to Eq. (89). The result

$$\bar{\alpha}_{C_2} = \frac{\delta k_m}{2E_m^2} \left(\frac{a_0}{R}\right) \frac{b}{(a^2 + b^2)} \int \int_S (p'_m)^2 \, dS \qquad (126)$$

is plotted in Fig. 12 vs the characteristic ratio M_b/δ for several modes for the Yang/Culick motor configuration. The dashed
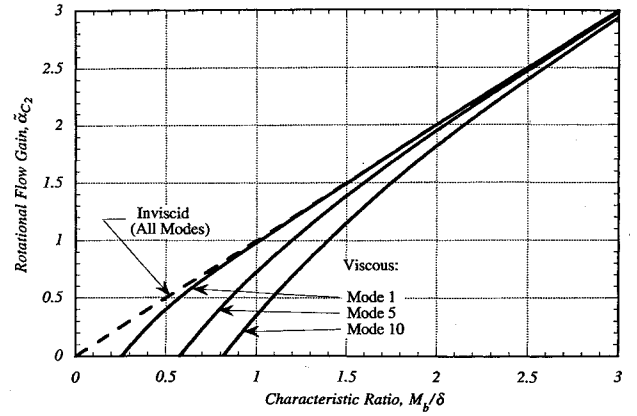
curve is the inviscid result for comparison. Notice that as the mode number increases, the range of validity for the inviscid solution is increased to higher values of M_b/δ. The viscous corrections significantly reduce the rotational flow gain effect for higher-order modes. Nonlinear stability calculations[14] involving superposition of acoustic modes must therefore be corrected to take account of the sensitivity of the effective surface gain to mode number for each component retained in the spectrum.

It is interesting to examine the limiting case for which the characteristic ratio M_b/δ grows larger. In the limit as the ratio of these two parameters increases indefinitely, one finds as $(M_b/\delta) \to \infty$

$$a \to 0 \qquad (127)$$

$$b \to \delta(k_m/M_b) = \delta/\lambda \qquad (128)$$

The dashed curve in Fig. 10 represents the limiting value of the imaginary part b. Notice that as M_b/δ increases, the viscous solution near the surface approaches the inviscid solution derived earlier. Therefore, the limiting case expressed in Eqs. (127) and (128) corresponds to the inviscid solution (Table 2) in the vicinity of chamber boundary. The simplified viscous results are valid for values of M_b/δ greater than about four, as indicated in the figure. For typical rocket motor thermodynamic conditions, this means that the limiting case corresponds to values of surface Mach number greater than about 0.0025. Reference to Table 1 shows that most actual rocket flows fall in this range.

For the limiting case just defined, the rotational flow gain correction is identical to the irrotational result. The dashed line in Fig. 12 corresponds to the inviscid limiting case. It should also be remarked that in the limit $M_b \to 0$, corresponding to an inert surface, the viscous model collapses to a well-known unsteady viscous solution, namely that of Stokes' second problem.[36]

It is apparent from the above considerations that the inviscid solution is applicable in most rocket applications. However, the viscous solution is easily applied, and if reliable thermodynamic data for the combustion gas flow is available Eq. (128) should be used to calculate the rotational flow driving correction. The flow-turning loss is unaffected by viscous forces and, therefore, depends only on the chamber radius, surface velocity, and mode shape.

VII. Discussion of Results

The analysis described in this article provides fresh insight into the effects of vorticity production and transport on combustion instability. The predicted unsteady flowfield results agree very well both with cold-flow experimental data and with numerical computations based on the full Navier–Stokes
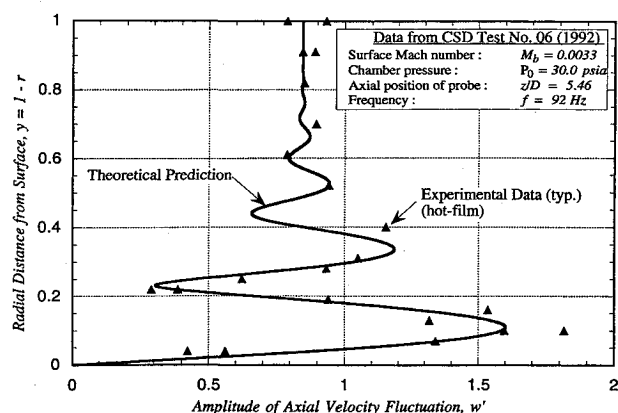
Fig. 13 Comparison of theoretical and experimental flowfield results.

equation. Figure 13 compares the results (inviscid) to the cold flow experimental data of Shaeffer and Brown.[16] The close agreement in magnitude, wavelength, and dependence on radial position establishes the validity of the theoretical results. The availability of an analytical solution provides both a direct physical connection to the parameters and a straightforward means to correct the previous (irrotational) approach to the stability computations.

The simple and highly useful inviscid solution is a limiting case of the more complete viscous analytical solution. The inviscid solution is the unsteady analogue of the Culick steady flow model for a cylindrically symmetric rocket flowfield. The viscous solution reduces to classical acoustic boundary-layer results when the surface mass flux approaches zero. It should be emphasized that the inviscid analytical model is valid throughout the combustion chamber for many rocket instability problems involving lower-order axial modes. The viscous solutions, based on an earlier analysis,[13] are only valid near the burning surface for lower-order modes. However, it happens that detailed information concerning the effects of rotational flow on system stability is required only near the injection surface. Extensive numerical calculations involving solution of the complete Navier–Stokes equations leads to identical conclusions.[19]

The appearance of a damping effect completely equivalent to the Culick flow-turning term is a significant finding. This has been accomplished in full three-dimensional form. Flow-turning is found to be the result of convective forces involving generation of unsteady vorticity at the burning surface. The volume integral of this convective acceleration effect reduces to a simple surface integration over boundaries with inward mass flux. This fully justifies Culick's earlier approach based on patching his one-dimensional results to the three-dimensional model.[8] The three-dimensional flow-turning loss exhibits all of the features of its one-dimensional counterpart. It is spatially dependent on the square of the unperturbed plane wave velocity mode shape (or square of the pressure gradient). It is directly proportional to the mean flow velocity at the surface, and inversely proportional to the chamber radius.

It is now quite easy to explain why the one-dimensional formulation gives rise to a damping effect not predicted in the irrotational, three-dimensional model. In the one-dimensional boundary value problem both steady and unsteady velocities are assumed by Culick to be normal to the surface at the propellant boundary. The impulsive change in gas particle movement from the normal fluctuating inflow to the axial oscillation brings about an energy loss related to a change in the total enthalpy, i.e., an "inelastic" effect as described by Culick.[7,8] This implies the presence of vorticity. But vorticity cannot, by definition, be involved explicitly in the one-dimensional model. However, it seems clear that some of the features of the actual three-dimensional motion must be

captured in this simplified model if the strong constraint of no-slip is imposed. Careful examination of the original one-dimensional computations shows that the equivalent of the rotational axial velocity correction arises in the stability surface integral as it does in Eq. (115), which is the reduced form of a volume integral. This velocity is equal and opposite to the acoustic crossflow velocity at the surface that would be present if slip were allowed. In other words, careful application of the one-dimensional mathematical protocol to the governing equations and boundary conditions gives rise, correctly, to the flow-turning effect, but without the physical clarity of the three-dimensional analysis. For example, it is not possible in a strictly one-dimensional calculation to see that viscous forces might not play an important role in the flow-turning damping. Effects such as vorticity propagation needed to accommodate the complicated boundary conditions associated with the actual flow interactions require a multidimensional format. Grappling with the far more complex three-dimensional mathematical problem pays off by yielding a more complete physical understanding of the flowfield, as well as identifying additional stability elements.

An important difficulty with the one-dimensional model is its inability to represent effects requiring a detailed model of the multidimensional flow near the boundaries. For example, the three-dimensional analysis shows that requiring satisfaction of realistic boundary conditions leads to a fluctuating radial velocity that modifies the system stability in a crucial way. Thus, the one-dimensional formulation gives an incomplete representation of the influence of rotational flow effects on system stability.

The strong rotational/acoustic coupling leads to a new driving effect that does not appear in a less complete analysis or one that neglects vorticity. The new destabilizing effect, rotational flow driving, represented by $\hat{\alpha}_{C_2}$ in Table 2, arises from an additional source of fluctuating velocity at the injection boundary created by the axial unsteady momentum defect or displacement effect. This radial "pumping" is the time-dependent analogue of the familiar radial velocity produced at the edge of a flat-plate boundary layer by the displacement effect.[36] It disappears only if the flow is assumed to be irrotational. The mean flow driving term does not. It is a coincidence that these two sources of acoustic energy lead to identical influence on system stability as shown in Table 2, Eqs. (88) and (89), for the inviscid limiting case. Viscous forces affect this destabilizing term only for cases involving lower burning rate propellants and high-frequency oscillations. The corresponding viscous effect is given in Eq. (126).

Ironically, Culick's earlier approach must now be applied in reverse. That is, all new terms must be added to the one-dimensional version of the stability code to correct it for vorticity transport effects that cannot be accounted for in a one-dimensional formulation. That is, both the one- and three-dimensional versions of the SSPP approach must be corrected as set forth herein. All important growth rate effects (except the particle damping) can be put in surface integral form; as such they are applicable to either the one- or three-dimensional formulation. Remember that the flow-turning volume integral, Eq. (91) can be replaced by the equivalent surface integral, Eq. (115).

Preliminary testing of the new stability theory has been carried out by comparison of standard SSPP predictions and stability predictions using a corrected version of the code in which the suggested modifications have been implemented. These stability predictions are plotted against the recent experimental measurements by Harris[37] in Fig. 14. A much improved predictive capability results from inclusion of the proposed revisions. The remaining scatter in Fig. 14 is of the sort associated with the uncertainties in the propellant admittance function measurements.

On the other hand, some researchers have reported acceptable agreement between experimental data and SSPP pre-
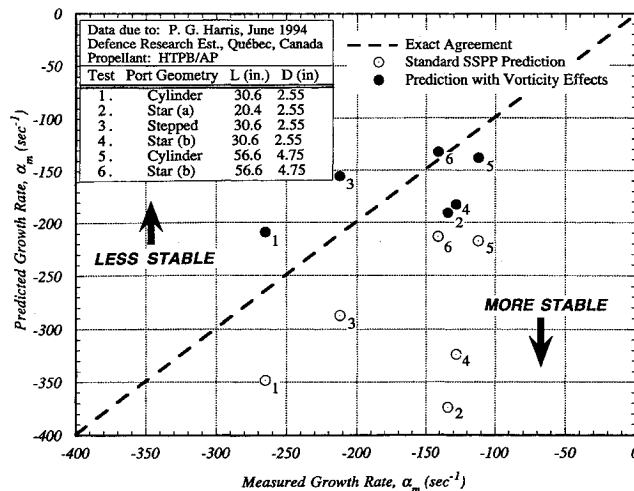
Fig. 14   Effect of rotational flow corrections on stability predictions.

dictions.[38] A detailed review of these cases is underway, and will be discussed in a subsequent publication. The strong dependence of the results on partial grain effects as emphasized in Table 3 may represent a partial explanation. Notice that the presence of slots, conocyls, or other gaps in the propellant grain have a significant influence on the results. Each of the new terms has a different dependence on grain length and axial position. The cancellations leading to Eq. (111) only occur for a truly full-length grain bonded to the case at both ends. Even rather short gaps, star-shaped port sections, or other grain features at the forward closure or nozzle end of the chamber have a significant effect on the stability predictions. Space restrictions preclude a more detailed discussion in this article.

Vortex shedding at intersegment gaps and other points of flow separation is an additional consequence of rotational flow interactions that leads to motor pressure oscillations. Previous analyses have assumed that vortical oscillations have negligible amplitude at the point of mean flow separation, the origin of large-scale vortex structures. These theories[28] have assumed that the disturbances grow spatially downstream from the origin of the strongly sheared mean flow. The amplitude of the traveling vortical waves at the origin is assumed to be zero. The results presented herein demonstrate that this is not the case. The oscillatory vorticity produced at burning surfaces upstream of the point of separation represents a powerful coupling to the acoustic field and sets the correct initial conditions in the spatial growth of large-scale vortex structures. The influence of this interaction on flow-driven pressure oscillations appears to be of major significance.[29] The vortex shedding coupling effect is strongest near the chamber velocity antinode as demonstrated experimentally by Brown[30] and others.

The theory described herein is, at the time of writing, being adapted for use in transverse mode applications. Several of the simplifications made in this article are not valid in those cases. A second paper emphasizing the influence of the rotational flow corrections on particle damping is also in preparation, since these are of vital importance in high-frequency applications. Work has already begun on extensions to nonlinear instability theory. The rotational flow corrections bring about significant modifications in finite amplitude stability analysis.

VIII.   Conclusions

The stability effects described in detail in this article were anticipated many years ago. For example, the thesis by Flandro[35] dealt with rotational flow effects involving motions parallel to a burning surface. Calculation of the flow interactions at the injection surface were similar in many ways to those worked out more completely in this article. That problem, involving generation of axial vortices in transverse motor instability, should be reworked in the light of the improved analysis of the flow/acoustics interactions presented herein. Work by Brown,[15] Glick[40,41] and their coworkers also indicated concern that rotational flow effects might be important.

Integration of vorticity effects into the combustion stability problem results in clarification of several issues left previously unresolved. In particular, the origin and physical significance of flow-turning are illuminated. Failure of flow-turning to appear in the earlier three-dimensional stability analyses was not due to the neglect of viscous forces as is frequently stated in the literature. It is more correct to say that failure to impose proper boundary conditions, namely the no-slip condition, in the multidimensional analysis led to considerable misunderstanding.

Flow-turning arises from interactions within the chamber caused when vorticity is created by the coupling between the steady and unsteady pressure gradients and the incoming radial flow. The vorticity is propagated mainly by convection, and to a lesser degree by viscous diffusion. There is transfer of energy from the pressure oscillations (acoustic field) to the vortical waves (vorticity field). It is in this interaction that the incoming oscillatory flow acquires the axial motion of the acoustic waves. This energy transfer accounts for the flow-turning loss.

The vorticity production is simply a consequence of the Crocco–Vazsonyi theorem, which makes it clear that vorticity will always be found in the flow whenever the total energy or the entropy is not uniform. In applying this theorem to the present case, it is only necessary to remember that such thermodynamic nonuniformities $[\rho(T\nabla s - \nabla h) = -\nabla p]$ are a direct consequence of the unsteady axial pressure gradient across the injection surface when longitudinal acoustic waves are present.

An unexpected finding is a new destabilizing effect related to the production of vorticity in the surface interactions. It is associated with work done in the process of inducing the spin of the incoming gas particles. This gain effect exactly cancels the flow-turning loss for some chamber configurations. Thus, the new results predict a less stable system behavior than previous theories of combustion instability.

Acknowledgment

References

[1]Lovine, R. L., Dudley, D. P., and Waugh, R. D., "Standardized Stability Prediction Method for Solid Rocket Motors," Vols. I, II, III, Aerojet Solid Propulsion Co., Air Force Rocket Propulsion Lab. TR 76-32, May 1976.

[2]Nickerson, G. R., Culick, F. E. C., and Dang, L. G., "Standardized Stability Prediction Method for Solid Rocket Motors Axial Mode Computer Program," Air Force Rocket Propulsion Lab. TR 83-017, Sept. 1983.

[3]Culick, F. E. C., "Acoustic Oscillations in Solid Propellant Rocket Chambers," Astronautica Acta, Vol. 12, No. 2, 1966, pp. 113–126.

[4]Cantrell, R. H., and Hart, R. W., "Interaction Between Sound and Flow in Acoustic Cavities: Mass, Momentum, and Energy Considerations," Journal of the Acoustical Society of America, Vol. 36, No. 4, 1964, pp. 697–706.

[5]Culick, F. E. C., "Stability of Longitudinal Oscillations with Pressure and Velocity Coupling in a Solid Propellant Rocket," Combustion Science and Technology, Vol. 2, No. 4, 1970, pp. 179–201.

[6]Beckstead, M. W., and Culick, F. E. C., "A Comparison of Analysis and Experiment for Solid Propellant Combustion Instabil-

ity," *AIAA Journal*, Vol. 9, No. 1, 1971, pp. 147–154.

[7]Culick, F. E. C., "The Stability of One-Dimensional Motions in a Rocket Motor," *Combustion Science and Technology*, Vol. 7, No. 4, 1973, pp. 165–175.

[8]Culick, F. E. C., "Stability of Three-Dimensional Motions in a Rocket Motor," *Combustion Science and Technology*, Vol. 10, No. 3, 1974, pp. 109–124.

[9]Price, E. W., "Velocity Coupling in Oscillatory Combustion of Solid Propellants," *AIAA Journal*, Vol. 17, No. 7, 1979, pp. 799, 800.

[10]Van Moorhem, W. K., "Flow Turning in Solid Propellant Rocket Combustion Stability Analysis," *AIAA Journal*, Vol. 20, No. 10, 1982, pp. 1420–1425.

[11]Magiawala, K. R., "Measurements of Energy Exchange Between Acoustic Fields and Nonuniform Steady Flow Fields," Ph.D. Dissertation, California Inst. of Technology, Pasadena, CA, 1978.

[12]Rao, N. X., and Van Moorhem, W. K., "Interactions of Particles with the Flow near the Burning Surface of a Solid Propellant Rocket," AIAA Paper 93-0110, Jan. 1993.

[13]Flandro, G. A., "Solid Propellant Acoustic Admittance Corrections," *Journal of Sound and Vibration*, Vol. 36, No. 3, 1974, pp. 297–312.

[14]Culick, F. E. C., and Yang, V., "Stability Predictions in Rockets," *Nonsteady Burning and Combustion Stability of Solid Propellants*, Vol. 143, Progress in Astronautics and Aeronautics, AIAA, Washington, DC, 1992, pp. 719–799.

[15]Brown, R. S., Blackner, A. M., Willoughby, P. G., and Dunlap, R., "Coupling Between Velocity Oscillations and Solid Propellant Combustion," AIAA Paper 86-0531, Jan. 1986.

[16]Shaeffer, C. W., and Brown, R. S., "Oscillatory Internal Flow Studies," United Technologies, Chemical Systems Div., 2060 FR, Aug. 1992.

[17]Vuillot, F., and Kuentzmann, P., "Flow Turning and Admittance Correction: An Experimental Comparison," *Journal of Propulsion and Power*, Vol. 2, No. 4, 1986, pp. 345–353.

[18]Flandro, G. A., "Effects of Vorticity Transport on Axial Acoustic Waves in a Solid Propellant Rocket Chamber," American Society of Mechanical Engineers Annual Meeting, San Francisco, CA, Dec. 1989.

[19]Flandro, G. A., and Roach, R. L., "Effects of Vorticity Production on Acoustic Waves in a Solid Propellant Rocket," Air Force Office of Scientific Research Final Rept., Contract AFOSR 90-0159, Dec. 1992.

[20]Vuillot, F., and Avalon, G., "Acoustic Boundary Layers in Large Solid Propellant Rocket Motors Using Navier-Stokes Equations," *Journal of Propulsion and Power*, Vol. 7, No. 2, 1991, pp. 231–239.

[21]Vuillot, F., "Numerical Computation of Acoustic Boundary Layers in Large Solid Propellant Space Booster," AIAA Paper 91-0206, Jan. 1991.

[22]Yang, V., and Roh, T. S., "Transient Combustion Response of Solid Propellant to Acoustic Disturbance in Rocket Motors," AIAA Paper 95-0602, Jan. 1995.

[23]Baum, J. D., "Investigation of Flow Turning Phenomenon; Effects of Frequency and Blowing Rate," AIAA Paper 89-0297, Jan. 1989.

[24]Sabnis, J. S., Giebeling, H. J., and McDonald, H., "Navier-Stokes Analysis of Solid Propellant Rocket Motor Internal Flows," *Journal of Propulsion and Power*, Vol. 5, No. 6, 1989, pp. 657–664.

[25]Culick, F. E. C., "Rotational Axisymmetric Mean Flow and Damping of Acoustic Waves in a Solid Propellant Rocket," *AIAA Journal*, Vol. 4, No. 8, 1966, pp. 1462, 1463.

[26]Dunlap, R., Willoughby, P. G., and Hermsen, R. W., "Flowfield in the Combustion Chamber of a Solid Propellant Rocket Motor," *AIAA Journal*, Vol. 12, No. 10, 1974, 1440–1442.

[27]Flandro, G. A., "Stability Prediction for Solid Propellant Rocket Motors with High-Speed Mean Flow," Air Force Rocket Propulsion Lab. TR, AFRPL TR-79, Jan. 1979.

[28]Flandro, G. A., "Vortex Driving Mechanisms in Oscillatory Rocket Flows," *Journal of Propulsion and Power*, Vol. 2, No. 3, 1986, pp. 206–214.

[29]Flandro, G. A., "Assessment of Flow Driven Pressure Oscillations in Shuttle ASRM Rocket Motor," Final TR, Contract WE10E3640N, Aerojet ASRM Div., Iuka, MS, Oct., 1993.

[30]Brown, R. S., Blackner, A. M., Dunlap, R., and Willoughby, P. G., "Vortex Shedding as a Source of Acoustic Energy in Segmented Rockets," *Journal of Spacecraft and Rockets*, Vol. 18, No. 4, 1981, pp. 312–319.

[31]Chu, B. T., and Kovasznay, L. S. G., "Non-Linear Interactions in a Viscous Heat-Conducting Compressible Gas," *Journal of Fluid Mechanics*, Vol. 3, No. 5, 1988, pp. 494–514.

[32]Temkin, S., *Elements of Acoustics*, Wiley, New York, 1981, pp. 421–424.

[33]Morse, P. M., and Ingard, K. U., *Theoretical Acoustics*, McGraw–Hill, New York, 1968, p. 279.

[34]Van Dyke, M., *Perturbation Methods in Fluid Mechanics* (annotated edition), The Parabolic Press, Stanford, CA, 1975.

[35]Cole, J. D., *Perturbation Methods in Applied Mathematics*, Blaisdell, Waltham, MA, 1968.

[36]Schlichting, H., *Boundary Layer Theory*, 7th ed., McGraw–Hill, New York, 1979, pp. 93–95.

[37]Harris, P. G., "Experimental Evaluation of One-Dimensional Design Technology for Linear Combustion Instability," AIAA Paper 94-3191, June 1994.

[38]Blomshield, F. S., Crump, J. E., Mathes, H. B., and Beckstead, M. W., "Stability Testing and Pulsing of Full Scale Tactical Motors," Vol. VI, Pts. A and B, Naval Weapons Center, China Lake, CA, Oct. 1991.

[39]Flandro, G. A., "Rotational Flow in Unstable Rocket Motors," Ph.D. Dissertation, Aeronautics Dept., California Inst. of Technology, Pasadena, CA, 1967.

[40]Wickliff, J. L., and Geyer, M. S., "On the Flow Reversal Condition in Combustion Instability," AIAA Paper 82-1221, June 1982.

[41]Glick, R. L., and Renie, J. P., "On the Nonsteady Flowfield in Solid Rocket Motors," AIAA Paper 84-1475, June 1984.